Geothermics 139 (2026) 103677

Contents lists available at ScienceDirect

Geothermics

journal homepage: www.elsevier.com/locate/geothermics

Thermal waters of the Western Bohemian Massif (Germany): geothermometry, origin and circulation

Simon Prause [a,*], Horst Kämpf [a], Gerhard Strauch [b], Alena Sophie Broge [a,c], Ferdinand Perssen [a], Jessica Alexandra Stammeier [a], Sascha Görne [d]

[a] GFZ Helmholtz Centre for Geosciences, Potsdam, Germany
[b] Helmholtz Centre for Environmental Research UFZ, Leipzig, Germany
[c] Georg-August-Universität, Göttingen, Germany
[d] Landesamt für Umwelt, Landwirtschaft und Geologie, Dresden, Germany

ARTICLE INFO

Keywords:
Deep geothermal energy
Water-rock interaction
Aqueous geochemistry
Geothermometry
Bohemian massif
Germany

ABSTRACT

The fault-bound basement-hosted geothermal systems of the Western Bohemian Massif (Germany) remain poorly constrained in terms of reservoir temperatures, circulation depths and recharge. Here, we present some of the first systematic constraints on these parameters based on a geochemical survey of regional thermal water, non-thermal groundwater and surface water, combining isotope techniques, a multi-method geothermometric approach and mixing calculations. Stable isotope ratios ($\delta^{18}O$ and $\delta^{2}H$) indicate that all studied thermal waters are derived from meteoric precipitation. The geothermal reservoirs of the region are identified as low-enthalpy "hot water type" systems with temperatures generally < 100 °C. The occurrence of local warm springs is linked to radiogenic heating in primarily granitic reservoirs at depth and migration of thermal water to the surface along long-lived permeable fault systems. Despite having interacted with similar reservoir lithologies at comparable temperatures, thermal waters exhibit pronounced hydrochemical variability in terms of composition, mineralization and extent of water-rock interaction. These differences primarily reflect structural characteristics of the individual geothermal systems, such as hydraulic openness and fault connectivity, which in turn affect recharge rates, residence times, extent of dilution with non-thermal groundwater and the supply of dissolved CO_2. Together, these results demonstrate that hydraulic connectivity and permeable fault architecture exert a first-order control on geochemical signatures in the geothermal systems of the Western Bohemian Massif and similar basement-hosted settings.

1. Introduction

Germany's geothermal resources are typically classified as low- to medium-enthalpy (commonly < 180 °C) and are predominantly used for space and district heating as well as balneological purposes (Agemar et al., 2014a). By contrast, recent official statistics (UBA/AGEE-Stat; Bundesnetzagentur; D-EITI) report that geothermal electricity generation contributed only ~0.20 TWh·yr^{-1} in 2023–2024, approximately corresponding to 0.04% of national electricity consumption. Previous geothermal exploration has primarily focused on sedimentary basins associated with permeable fault systems, such as the North German Basin, the Upper Rhine Graben and the southern Molasse Basin, where geothermal gradients in excess of 40 °C·km^{-1} have been observed in some cases (Agemar et al., 2012, 2014a, 2014b; Franz et al., 2018; Frey et al., 2022; Moeck et al., 2019; Suchi et al., 2014; Weber et al., 2020). More recently, however, the Western Bohemian Massif in SE Germany has attracted increased interest with regard to geothermal development, because the crust in this area is enriched in radioactive elements to a depth of up to ~15 km, leading to locally increased radiogenic heat production of up to 4–10 μW·m^{-3}, particularly in proximity to local granites, monzonites and syenites (de Wall et al., 2019; Förster et al., 2018; Förster and Förster, 2000). Temperature and heat flow modeling as well as 3D seismic investigations of the Elbe Zone and Gera-Jáchymov fault zone in Southern and Southwestern Saxony indicate that temperatures of 120 °C to >150 °C may be achieved at 3–6 km depth in local granitic complexes (Förster et al., 2018; Hloušek et al., 2015; Lüschen et al., 2015; Lüschen and Schulz, 2014).

While these early investigations have primarily targeted

* Corresponding author.
E-mail address: simon.prause@proton.me (S. Prause).

https://doi.org/10.1016/j.geothermics.2026.103677
Received 6 January 2026; Received in revised form 23 March 2026; Accepted 23 March 2026
Available online 28 March 2026

petrothermal systems with the goal of evaluating their potential for Enhanced Geothermal System (EGS) development, the region also hosts a number of hydrothermal systems feeding several warm springs, some of which are used by local spas. Although some investigations on the hydrochemistry of regional thermal water have been carried out in the past, most available research on geothermal resources has either remained unpublished or focused on balneological and therapeutic applications (e.g., von Storch, 1998). By contrast, little concrete information on reservoir temperatures, origin, circulation and residence times of the various geothermal systems in the region is currently available.

As part of the E4Geo research project, the local state authority of Saxony has commissioned an investigation of the regional fault-bound geothermal systems of the western margins of the Bohemian Massif, with a specific focus on determining the geothermal potential of the SW-Vogtland region between the cities of Plauen, Oelsnitz and Hof. This paper presents the results of an early-stage geochemical survey constraining likely reservoir temperatures, circulation depths, recharge areas and relative residence times of the local geothermal systems based on the chemical and isotopic composition of regional surface, ground- and thermal water. Our geochemical reconnaissance is intended to contribute to closing the current research gap on the regional fault-bound geothermal resources of the area. New insights on reservoir conditions and circulation will aid in making informed decisions regarding a potential geothermal project in the SW-Vogtland region while also contributing to the sustainable use of currently exploited geothermal resources in the wider Western Bohemian Massif.

2. Geological setting

As part of the Saxothuringian Zone, the Ore Mountains and a number of other integral members of the Variscan belt, such as the Vogtland and the Fichtel Mountains, are overlain by the Tepla-Barrandian Domain along its SE margin (Franke, 1989). The area constitutes a classical metallogenetic province, rich in granitic rocks and vein-ore deposits (Sn-polymetallic, U-carbonate, fluorite-baryte and Bi-Co-Ni-Ag). The Saxothuringian Zone is predominantly composed of orthogneisses of Proterozoic to early Paleozoic age emplaced during the Cadomian orogeny (Collett et al., 2020; Kroner et al., 2007; Tichomirowa et al., 2001) and Variscan metamorphosed volcano-sedimentary sequences (protolith ages ranging from Cambrian to Devonian) composed of phyllites, micaschists and paragneisses, intercalated with by meta-conglomerates, quartzites, amphibolites and marbles (Mingram, 1998; Rötzler and Plessen, 2010; Schulz and Krause, 2024). The metamorphic rock sequences were intruded by granitoids over the course of a late Variscan (ca. 325–315 Ma) and a post-Variscan (ca. 305–296 Ma) magmatic period (Burisch et al., 2019; Gottesmann et al., 2017; Tichomirowa et al., 2025).

Thermal fluid circulation in the lithosphere of the study area has been documented in the Mesozoic and the Cenozoic, leading to the genesis of Mesozoic hydrothermal ore deposits in Europe, associated with the tectonic evolution of the Tethys-Atlantic-Caribbean rift system during the breakup of Pangaea (Burisch et al., 2022). The three study areas considered in this work are part of the northern shoulder of the Cenozoic Eger Rift (Andreani et al., 2014; Ulrych et al., 2011). Volcanic and hydrothermal activity from Middle Pleistocene to date was documented in the Western part of the Eger Rift (Kämpf et al., 2007; Mrlina et al., 2009; Vylita et al., 2007).

2.1. Central Ore Mountains

Morpho-tectonically the Central Ore Mountains Anticlinal Area is divided into two blocks by the N-S striking Annaberg-Tepla fault zone: the Marienberg high and the Annaberg high (Andreani et al., 2014). The Ehrenfriedersdorf granites intruded the metamorphic basement of the study area as part of the Central Ore Mountains sub-pluton approximately 312–324 Ma ago (Hoth et al., 1991; Romer et al., 2007), typifying them as late Variscan. The Georgsquelle spring is situated atop a 79 m deep borehole drilled in 1919 located at the ca. 40 km long and 500 m wide NW-SE striking Wiesenbad fault zone, which is partially mineralized with quartz, baryte and fluorite (Kuschka, 1997, 2002; von Storch et al., 2000). The Warmbad warm spring has been known since 1284 and is located at the “Neugeboren Kindlein” fault zone, part of the NW-SE striking Warmbad-Chomutov fault zone (von Storch et al., 2000).

2.2. SW-Vogtland

In the SW-Vogland area (Fig. 1), the intersection of NE-SE and NNW-SSE striking faults acts as a fluid conduit for regional ground- and thermal water (Bräuer et al., 2008; Kämpf, 1982). The SW-Vogtland area belongs to the NE-SW striking Vogtland Slate Mountains, characterized by three NW-SE directed Horst structures (from NE to SW: Netzschkau Horst, Tauschwitz Horst and Triebel Horst), made up of Silurian and Devonian volcanic rocks along their flanks and Ordovician metasediments at the top (Schwan, 1959). Two apical intrusions form the concealed granite massif of Eichigt-Schönbrunn, a peraluminous Si-rich biotite monzo- to syenogranite of A-type affinity (Gottesmann et al., 2017; Schützel and Hösel, 1962) (Fig. 1). The Schönbrunn granite has been dated at 307 ± 4 Ma (Schulz and Krause, 2024).

Fault tectonics of the study area are characterized by the intersection of NW-SE directed faults at the flanks of the horst-structures with N-S directed faults of the Regensburg-Leipzig-Rostock zone (RLRZ) (Bankwitz et al., 2003). The RLRZ is seismically active (Fischer et al., 2014). The driving force of the earthquake swarm seismicity in the region most likely is magmatic and fluid activity in the lower crust and lithospheric mantle (Bräuer et al., 2003, 2011).

The warm spring of Schönbrunn has been known since 1973 when mining on the 453 m level of the Schönbrunn-Bösenbrunn fluorite mine intersected a permeable fault system formed by the intersection of NW-SE with NNW-SSE striking faults. After the cessation of fluorite mining in 1991, the Schönbrunn mine underwent flooding in December 1997. About 5 km west of Schönbrunn, the artesian warm spring of Neumühle, which is connected to thermal water-bearing faults hosted in diabase at 771 m depth, was established as an unintended side effect during a 1176 m deep exploratory drilling project by the uranium industry of the former G.D.R. in 1960 (Schützel and Hösel, 1962).

2.3. Fichtel Mountains

The Fichtelgebirge-Paleozoic (Fig. 1) is tectonically formed as a NE-SW striking antiform and part of the Saxothuringian upper plate of the Variscan orogeny above the SE-dipping subduction zone (Schäfer et al., 2000). The 1835 m deep borehole of the Siebenquell warm spring was drilled in 2013, penetrating late and post Variscan granites of the Fichtel Mountains/Smirciny pluton, which intruded the local metamorphic basements between 326 and 321 Ma (Förster et al., 2008; Röckel and Stober, 2017; Siebel et al., 2003). Temperatures of 53.4 °C have been measured at the bottom of the Siebenquell borehole (Röckel and Stober, 2017). According to gravimetric measurements and modeling, the thickness of the western and central part of the granite massif is estimated as 3000 m (Hecht and Vigneresse, 1999). Carbonate-related metallic and non-metallic mineralization in the granitic rocks of the Fichtel Mountains pluton hints at intense hydrothermal activity in the Mesozoic and Cenozoic (Burisch et al., 2022; Dill and Kolb, 2019).

The well of the Radonquelle cold spring, located at a horizontal distance of 500 m to the north of the Siebenquell warm spring is approximately 71.3 m deep and situated in extensively weathered granite (Röckel and Stober, 2017). U/Th decay in the granitic host rock causes the Radonquelle spring water to be enriched in dissolved radon gas (Röckel and Stober, 2017), which is thought to be beneficial for the treatment of inflammation and chronic pain. Hence, the Radonquelle spring water is used for balneotherapy of rheumatic and joint conditions

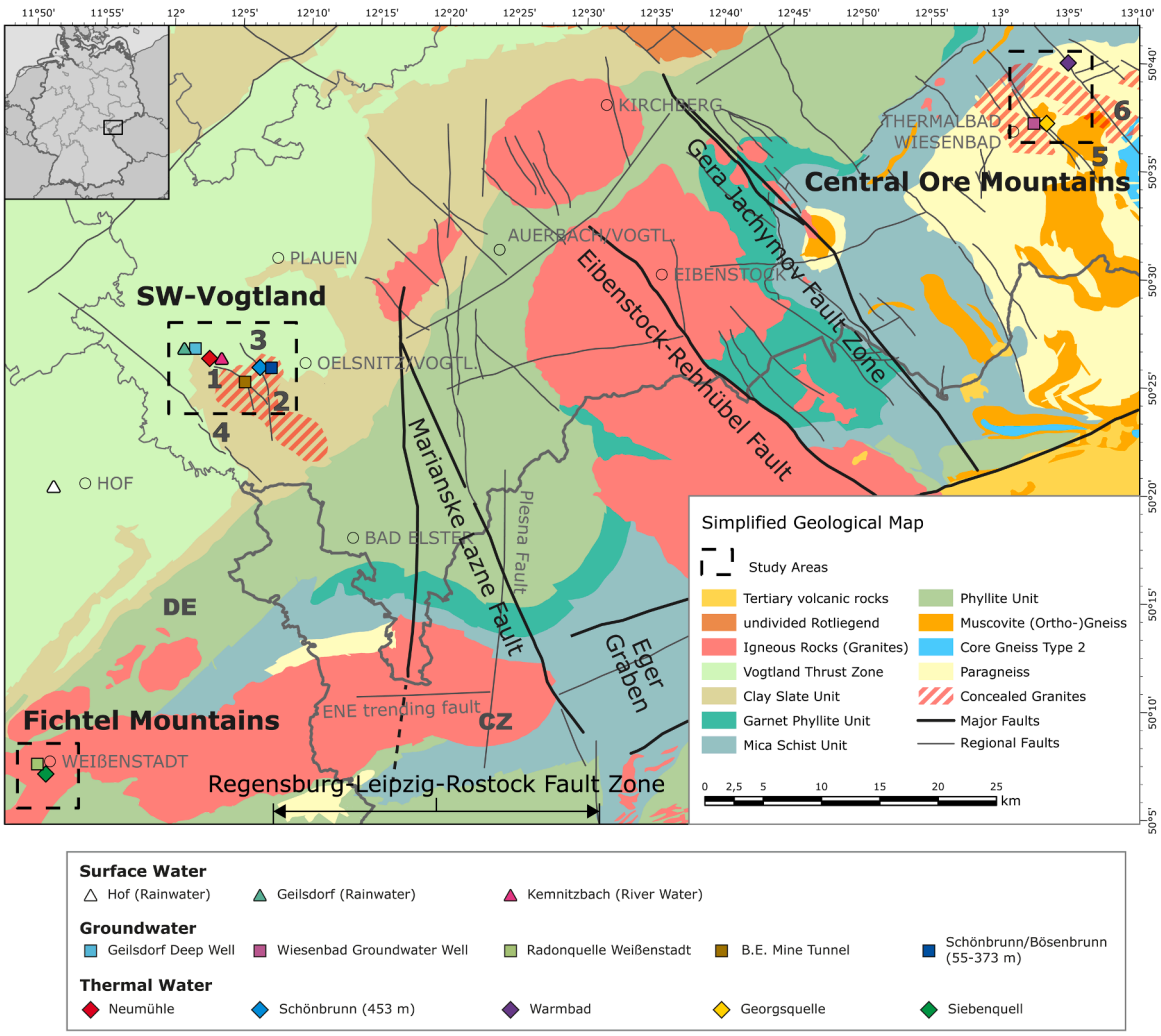

Fig. 1. Geological map showing the locations of the three study areas and sampling points of ground-, thermal- and surface water included in this study. Numbers 1–6 refer to the following regional faults: 1: Bösenbrunn Fault, 2: Triebeler Pfahl Fault, 3: Schönbrunn Fault, 4: South Vogtland Cross Fault, 5: Wiesenbad Fault, 6: Warmbad-Chomutov Fault.

by a local spa.

3. Methods and data

All data used in this work, including detailed descriptions on sampled locations and sampling dates are available in a dedicated open access data publication (Prause et al., 2026). The dataset includes both hydrochemical and isotopic measurements performed regional surface water, groundwater and thermal water of the Western Bohemian Massif from a field survey in 2022–2024 as well as legacy data. Due to flooding of the mine shaft, all information on the ground- and thermal water from the Schönbrunn/Bösenbrunn fluorite mine is limited to legacy data only and therefore any possible changes that may have occurred in the hydrological system since 1996 cannot be accounted for by our current dataset. Information on individual locations, including geographic coordinates, surface elevation, water type and additional comments on each location are summarized in Table 1.

3.1. Sampling and analysis

Sampling and analysis were carried out as part of our field survey conducted between 2022 and 2024 (Prause et al., 2026). Temperature, pH and electrical conductivity were measured in the field using a Xylem Inc. WTWQ Multi 3420 instrument. Bicarbonate concentrations were also determined in the field by acid titration using a Sigma-Aldrich Supelco MQuant® Carbonate Hardness test kit. Water samples were degassed through stirring and shaking prior to determining HCO_3 concentrations. Water samples for major cation and anion analysis were collected in 50- and 75-mL polyethylene bottles, respectively. Samples for cation analysis were filtered and acidified to ~pH 2 using 65% HNO_3. For transport, samples were stored in a portable cooler. Anion and cation concentrations were analyzed at the Elements and Minerals of the Earth (ElMiE) Laboratory at the GFZ Helmholtz Centre for Geosciences, Potsdam. Anion concentrations were measured by Ion Chromatography (IC) on a Thermo Fisher Scientific ICS-3000 with a flowrate of 0.38 mL min^{-1} and using 1.4 mM KOH as eluent. For samples with Cl^- concentrations of > 1 g L^{-1}, Cl^- and SO_4^{2-} were measured after dilution and the remaining anions were measured separately as described above after removal of Cl^- using Thermo Fisher Scientific OnGuard II Ag/H cartridges. Cation concentrations were determined by Inductively Coupled Plasma Optical Emission Spectroscopy (ICP-OES) using a 5110 spectrometer with Vertical Dual View configuration (Agilent, USA) after dilution of samples with ultrapure HCl. Further information on analytical protocols is available in our open access data publication (Prause et al., 2026). Samples for isotopic analyses of $\delta^{18}O$, $\delta^{2}H$, and ^{3}H were stored in 10 ml glass bottles. Stable isotope ratios $\delta^{18}O$ and $\delta^{2}H$ were measured by the Hydroisotop GmbH, Schweitenkirchen, Germany by Cavity Ringdown Spectroscopy (CRDS) using Standard Mean Ocean

Table 1
Overview of locations and studied water (see Prause et al., 2026 for additional details).

Location	Coordinates	Surface Elevation (MASL)	Water Type	Comment
Georgsquelle	50.619185 N 13.043338 E	430	Thermal Water	Sampled from warm spring; thermal water used by local spa
Neumühle	50.421307 N 12.049495 E	380	Thermal Water	Sampled from warm spring
Schönbrunn (453 m)	50.406427 N 12.130732 E	475	Thermal Water	Subterranean warm spring located on the 453 m level of a local abandoned fluorite mine; only legacy data from 1994–1996 available due to flooding of the mine in 1997
Siebenquell	50.095177 N 11.873249 E	620	Thermal Water	Sampled from a well on the premises of a local spa center; water cooled from ~53 °C at the borehole outlet to ~32 °C at the sampling point
Warmbad	50.666063 N 13.08381 E	460	Thermal Water	Sampled from warm spring; thermal water used by local spa
Brüder Einigkeit Mine Tunnel	50.399317 N 12.100794 E	419	Groundwater	Sampled from surface discharge point, where mine effluent drains into the Triebel River
Geilsdorf Deep Well	50.422684 N 12.045409 E	424	Groundwater	Sampled from an artesian groundwater well with a depth of ~50 m in Weischlitz near Geilsdorf
Radonquelle Weißenstadt	50.098722 N 11.870218 E	616	Groundwater	Sampled from cold spring; water used by local spa
Schönbrunn/ Bösenbrunn (70–373 m)	~50.406427 N ~12.130732 E	~475	Groundwater	Mine water from the 70–373 m levels of the local abandoned fluorite mine; only legacy data from 1996 available for the 70 m level; only legacy data from 1973–1978 available for the 133–373 m levels; exact coordinates vary by sampling point but lie in close horizontal proximity to those of the Schönbrunn (453 m) thermal water
Wiesenbad Groundwater Well	50.618518 N 13.044028 E	445	Groundwater	Sampled from a well located at a horizontal distance of ca. 90 m from the Georgsquelle warm spring.
Geilsdorf (Rainwater)	50.422684 N 12.045409 E	424	Surface Water	Sampled near the Geilsdorf Deep Well in Weischlitz near Geilsdorf; only isotope data available
Hof (Rainwater) – DWD 2022	50.312537 N 11.875915 E	564	Surface Water	Sampled at the DWD weather station in Hof; only isotope data available
Kemnitzbach (River Water)	50.421205 N 12.049891 E	378	Surface Water	Sampled from the Kemnitzbach creek near the Neumühle warm spring; only isotope data available

Water (SMOW) as reference standard. Tritium concentrations (in TU) were measured by the IAF Radioökologie GmbH, Radeberg, Germany using Liquid Scintillation Counting (LSC) after electrolytic preconcentration.

3.2. Estimation of reservoir temperatures by empirical geothermometry

Empirical geothermometers applied in this study included the silica geothermometers for quartz and chalcedony (Fournier, 1977), four different Na-K geothermometers (Arnórsson et al., 1983; Fournier, 1979; Giggenbach, 1988; Santoyo and Díaz-González, 2010), the K-Mg geothermometer (Giggenbach, 1988), the Na-K-Ca geothermometer (Fournier and Truesdell, 1973) and the Na-K-Ca-Mg geothermometer (Nieva and Nieva, 1987). An overview of these geothermometers and relevant equations is provided in Table 2.

3.3. Estimation of reservoir temperatures by multicomponent equilibrium geothermometry

Multicomponent equilibrium geothermometry (MEG) (Reed, 1982; Reed and Spycher, 1984) was performed using the PHREEQC geochemical software (Parkhurst and Appelo, 1999). A detailed outline of the calculations involved, including an example PHREEQC script is provided in the supplement (S.1). In brief, the MEG method tests for the simultaneous equilibration of multiple primary or secondary minerals at a specific temperature by calculation of their saturation indices SI, defined as

$$SI = \log\left(\frac{Q}{K}\right) \quad (1)$$

where Q is the reaction quotient of a mineral's dissolution/precipitation reaction and K is the temperature dependent equilibrium constant of the same reaction. A mineral is saturated in solution, and therefore "in equilibrium" with a thermal water, if $Q = K$ and therefore $SI = 0$. Because the attainment of this equilibrium state is kinetically driven, the equilibration of an entire mineral assemblage typically requires prolonged water-rock interaction. Thus, the temperature indicated by the simultaneous equilibration of several mineral phases is assumed to reflect the temperature in the geothermal reservoir.

Thermodynamic data, including equilibrium constants of mineral formation reactions at variable temperature needed for the calculation of saturation indices, were taken from the carbfix.dat database (Voigt et al., 2018). Because of a lack of drill core samples and mineralogical data, the exact mineral assemblage at depth is presently unknown for the geothermal systems included in this study. Therefore, selection of possible equilibrium minerals was informed both by available mineral phases specified in the carbfix.dat database and by existing information on mineral parageneses commonly encountered in terrestrial low-temperature geothermal systems, particularly those associated with granite. Such parageneses commonly include silica (chalcedony and quartz), calcite, smectites, kaolinite, clinochlore, various zeolites, muscovite and feldspars (Browne, 1978; Gottesmann et al., 2017; Li et al., 2018, 2020; Mao et al., 2022; Ngo et al., 2016; Parneix and Petit, 1991; Savage et al., 1987; Yasuhara et al., 2011).

Since our data did not contain information on Al, its activity was estimated using the FixAl method developed by Pang and Reed (1998), assuming equilibrium with kaolinite, due to its widespread abundance and rapid equilibration even at low temperatures (Murray, 1988). Alternate solutions using adjusted Mg activities derived by the same method and assuming equilibration with clinochlore-14 Å were tested as well. To avoid overcorrection, adjustment of Mg activity was only considered justified if its inclusion in the model increased the number of equilibrium phases by at least one or if no feasible solution could be found without it. Possible dilution of thermal water along its flow path between reservoir and surface was accounted for by making calculations with a range of input concentrations scaled by application of a dilution factor (e.g., Fowler et al., 2018; Hou et al., 2019; Pang and Reed, 1998). Geothermal reservoir water is typically saturated with respect to calcite (Arnórsson, 1989) and supersaturation of calcite is therefore commonly interpreted as a pH effect caused by CO_2 degassing (Palandri and Reed, 2001). Therefore, if any calcite supersaturation was observed, this was

Table 2
Overview of empirical geothermometers applied in this study and necessary equations for their use.

Geothermometers	Equations
Silica:	
Fournier (1977)	$\text{Chalcedony}: T[^\circ C] = \frac{1032}{4.69 - \log SiO_{2,mg/kg}} - 273.15$
	$\text{Quartz (conductive)}: T[^\circ C] = \frac{1309}{5.19 - \log SiO_{2,mg/kg}} - 273.15$
	$\text{Quartz (adiabatic)}: T[^\circ C] = \frac{1522}{5.75 - \log SiO_{2,mg/kg}} - 273.15$
Na-K:	
Fournier (1979)	$T[^\circ C] = \frac{1217}{\log\left(\frac{Na_{ppm}}{K_{ppm}}\right) + 1.483} - 273.15$
Arnórsson and Gunnlaugsson (1983)	$T[^\circ C] = \frac{933}{\log\left(\frac{Na_{ppm}}{K_{ppm}}\right) + 0.993} - 273.15$
Giggenbach (1988)	$T[^\circ C] = \frac{1390}{\log\left(\frac{Na_{mg/kg}}{K_{mg/kg}}\right) + 1.75} - 273.15$
Santoyo and Díaz-González (2010)	$T[^\circ C] = \frac{876.3}{\log\left(\frac{Na_{mg/L}}{K_{mg/L}}\right) + 0.8775} - 273.15$
K-Mg:	
Giggenbach (1988)	$T[^\circ C] = \frac{4410}{14 - \log\left(\frac{K^2_{mg/kg}}{Mg_{mg/kg}}\right)} - 273.15$
Na-K-Ca:	
Fournier and Truesdell (1973)	$a = \log\left(\frac{Na_{mol/kg}}{K_{mol/kg}}\right) + \frac{1}{3} \times \log\left(\frac{\sqrt{Ca_{mol/kg}}}{Na_{mol/kg}}\right)$
	$b = \log\left(\frac{Na_{mol/kg}}{K_{mol/kg}}\right) + \frac{4}{3} \times \log\left(\frac{\sqrt{Ca_{mol/kg}}}{Na_{mol/kg}}\right)$
	$T_1[^\circ C] = \frac{10^3}{(a + 2.2405) : 1.6473} - 273.15$
	$T_2[^\circ C] = \frac{10^3}{(b + 2.2405) : 1.6473} - 273.15$
	$\text{If } \log\left(\frac{\sqrt{Ca_{mol/kg}}}{Na_{mol/kg}}\right) < 0: \ T = T_1$
	$\text{Else if } \log\left(\frac{\sqrt{Ca_{mol/kg}}}{Na_{mol/kg}}\right) > 0 \text{ and } T_2 > 100: \ T = T_1$
	$\text{Else}: T = T_2$
Na-K-Ca-Mg:	
Nieva and Nieva (1987)	$TMEQ = Na_{meq/L} + K_{meq/L} + Ca_{meq/L} + Mg_{meq/L}$
	$\%Mg = \frac{Mg_{meq/L}}{TMEQ} \times 100$
	$T_1[^\circ C] = \frac{1178}{\log\left(\frac{Na_{mol/kg}}{K_{mol/kg}}\right) + 1.239} - 273.15$
	$T_2[^\circ C] = \frac{16000}{3\log\left(\frac{Na_{mol/kg}}{K_{mol/kg}}\right) + 3\log\left(\frac{Ca_{mol/kg}}{Na^2_{mol/kg}}\right) - \log\left(\frac{Mg_{mol/kg}}{Na^2_{mol/kg}}\right) + 44.67} - 273.15$
	$T_3[^\circ C] = \frac{11140}{6\log\left(\frac{Na_{mol/kg}}{K_{mol/kg}}\right) + \log\left(\frac{Mg_{mol/kg}}{Na^2_{mol/kg}}\right) + 18.3} - 273.15$
	$T_4[^\circ C] = \frac{10080}{5\log\left(\frac{Na_{mol/kg}}{K_{mol/kg}}\right) + 2\log\left(\frac{Ca_{mol/kg}}{Na^2_{mol/kg}}\right) - \log\left(\frac{Mg_{mol/kg}}{Na^2_{mol/kg}}\right) + 16.65} - 273.15$
	$\text{If } TMEQ > 8 \text{ and } \%Mg \leq 3.5 \text{ and } T_1 > 125^\circ C: T = T_1$
	$\text{Else if } \frac{\sqrt{Mg_{mol/kg}}}{Na_{mol/kg}} > 1.7: \ T = T_2$
	$\text{Else if } \frac{\sqrt{Ca_{mol/kg}}}{Na_{mol/kg}} \leq 2.6: T = T_3$
	$\text{Else}: T = T_4$

corrected for by adding a sufficient amount of CO_2(g) to the model to equilibrate calcite in the reservoir (Palandri and Reed, 2001; Pang and Reed, 1998).

3.4. Mixing calculations using silica enthalpy

Based on the assumption that a sampled thermal water represents a mixture of a deep hot water (*HW*) and a cold groundwater (*CW*) from shallower depth, reservoir temperatures can be estimated graphically by plotting the enthalpy of both thermal and groundwater vs dissolved silica contents according to the method of Truesdell and Fournier (1977). If no boiling is assumed to have taken place prior to mixing, a line is projected through *CW* and the mixed water (*MW*) onto the quartz solubility curve, which can be constructed based on the data provided in

Table 1 of Fournier and Truesdell (1974). The intersect of this line with the quartz solubility curve reflects the enthalpy and silica content of *HW*. The fraction F_{HW} of the hot water in the mixture is given through application of the lever rule according to the ratios of the distances between *CW* to *MW* and *CW* to *HW*:

$$F_{HW(no\ steam\ loss)} = \frac{CW \rightarrow MW}{CW \rightarrow HW} \quad (2)$$

Alternatively, if adiabatic cooling is assumed to have occurred, a line is projected parallel to the x-axis onto the maximum steam loss curve from the point where the mixing line between *CW* and *MW* intersects with the enthalpy of the system during steam loss (Truesdell and Fournier, 1977), equivalent to ~100.1 cal·g^{-1} if a boiling point of 100 °C is assumed (Fournier and Truesdell, 1974). The intersect of the projected line with the maximum steam loss curve marks the enthalpy of *HW* before boiling. From there, another line is projected parallel to the y-axis onto the quartz solubility curve, with the intersect providing the original silica content of *HW* before steam loss. The value of F_{HW} after boiling is then determined from the distances *CW* to *MW* and *CW* to the boiling point *BP* as:

$$F_{HW(steam\ loss)} = \frac{CW \rightarrow MW}{CW \rightarrow BP} \quad (3)$$

3.5. Estimation of circulation depths and recharge elevations

In geothermal systems, hydrochemical and isotopic data record useful information that may be used in estimating both approximate circulation depth and recharge elevation (e.g., Mao et al., 2021). The circulation depth d_C is estimated according to:

$$d_C = (T_{res} - T_0)/\nabla T + d_0 \quad (4)$$

where T_{res} is the temperature of the geothermal reservoir, T_0 is the temperature of the constant temperature zone, which remains unaffected by seasonal changes throughout the year, d_0 is the depth of the bottom boundary of the constant temperature zone and ∇T is the local geothermal gradient. A value of $T_0 = 9$ °C based on the available information from both the GeotIS database and Förster and Förster (2000) was used for all calculations. For Neumühle and Schönbrunn ∇T was assumed as 29 °C·km^{-1} based on regional temperature measurements with a long shut-in time of 1248 h as published by Förster and Förster (2000) and d_0 was set to 55 m, based on Hofmann et al. (2021). This temperature is close to the average surface temperature in Germany of ~8.2 °C (Agemar et al., 2014a). For Warmbad, Georgsquelle and Siebenquell, values for ∇T and d_0 (Table 3) were estimated based on available data from the Geothermal Information System for Germany ("GeotIS") of the Leibniz Institute for Applied Geophysics (LIAG) (https://www.geotis.de/geotisapp/geotis.php) (Agemar et al., 2012, 2014b).

The recharge elevation h_R was estimated from the following equation:

$$h_R = \left(\delta^{18}O_{tw} - \delta^{18}O_{sw}\right)/\nabla\delta^{18}O + h_{sw} \quad (5)$$

where $\delta^{18}O_{tw}$ and $\delta^{18}O_{sw}$ are the stable oxygen isotopic signatures of thermal and surface water relative to SMOW in ‰, respectively, $\nabla\delta^{18}O$ is the isotopic elevation gradient in local precipitation and h_{sw} is the elevation where the surface water was sampled. For $\delta^{18}O_{tw}$, an average value for each thermal water was used (Table 3). The value for $\delta^{18}O_{sw}$ was estimated based on monthly average $\delta^{18}O$ precipitation values collected at an elevation of $h_{sw} = 564$ m at the weather station of the German Meteorological Service ("Deutscher Wetterdienst, DWD") at Hof in 2022 (Prause et al., 2026; Schmidt et al., 2020; Koeniger et al., in prep.). The $\delta^{18}O$ values from Hof were weighted by monthly precipitation amount retrieved from the DWD Climate Data Center (CDC) database (https://cdc.dwd.de/portal/), yielding a value of −9.1 ‰ for $\delta^{18}O_{sw}$. The elevation gradient $\nabla\delta^{18}O$ for Germany is about −0.47 ‰·100^{-1}·m^{-1} (Stumpp et al., 2014).

4. Results

4.1. Hydrochemistry

Table 4 lists representative average chemical compositions, temperatures, pH and EC of ground- and thermal water included in this study. To maintain consistency and mitigate the potential effects of compositional changes that may have occurred over longer time periods, only measurements conducted during the recent GFZ field survey in 2022–2024 (Prause et al., 2026) are included in the listed averages for most locations.

Non-thermal groundwater had temperatures between ~9.6 and 18.4 °C and typically was either of neutral or weakly alkaline pH, with the only exception being the water from the Radonquelle cold spring in the Fichtel Mountains with a slightly acidic pH of 5.8. The groundwaters from the Radonquelle cold spring and the Brüder Einigkeit Mine Tunnel were of a mixed Na-Ca-Cl type (Fig. 2). The shallow groundwaters from the Geilsdorf Deep Well, the Schönbrunn/Bösenbrunn mine from ~70–173 m and the Wiesenbad Groundwater Well were all of the Ca-HCO_3 or mixed Na-Ca-HCO_3 type (Fig. 2). The composition of the Schönbrunn/Bösenbrunn mine water changed with depth, showing increasing dominance of Na over Ca and Cl over HCO_3, resulting in a Na-Cl type water at depths ≥ 253 m (Fig. 2).

All thermal water included in this study originates from warm springs with temperatures ≤ 54 °C and generally circumneutral to weakly alkaline pH. Measured compositions of thermal water based on samples from the 2022–2024 field survey were mostly stable over time for studied locations, except for the Siebenquell thermal water, which exhibited highly variable K concentrations of < 1 to 2.5 mg·L^{-1} (Prause et al., 2026). Both the Neumühle and Schönbrunn (453 m) thermal waters were highly mineralized with a total dissolved solids (TDS) content of 5755 and 2410 mg·L^{-1}, respectively, which was one order of magnitude higher than for the other thermal waters, whose TDS ranged between 309–539 mg·L^{-1}. The thermal waters of SW-Vogtland and the Fichtel Mountains, including Neumühle, Schönbrunn (453 m) and Siebenquell were Cl-dominated with both the Schönbrunn (453 m) and Siebenquell thermal water being classified as Na-Cl type, whereas the Neumühle warm spring was found to have undergone evolution from a Na-Cl type in June 1961 to a Ca-Cl type in November 1961 to 2024 (Fig. 2). This change in hydrochemical facies was accompanied by increasing mineralization of the Neumühle thermal water, primarily caused by rising concentrations of Ca, Mg, Na, SO_4 and Cl (Fig. 3). Bicarbonate remained largely unaffected by this process. The thermal waters from the Central Ore Mountains were rich in Ca and HCO_3 and included the mixed Na-Ca-HCO_3 type water from Warmbad and the Na-HCO_3 type water from Georgsquelle (Figs. 2 and 3).

4.2. Isotopes of water ($\delta^{18}O$, $\delta^{2}H$, ^{3}H)

Tritium contents of "modern" surface water in the studied regions ranged between 2.2 to 13.7 TU (Table 5). Analyzed surface water had

Table 3
Average $\delta^{18}O$ values of thermal water and local geothermal gradients used for estimating circulation depths and recharge elevations according to Eqs. (4) and (5).

Location	$\delta^{18}O_{tw}$ (‰)	∇T (°C·km^{-1})	d_0 (m below surface)
Neumühle	−10.4	29	55
Schönbrunn (453 m)	−10.5	29	55
Warmbad	−10.0	29	20
Georgsquelle	−10.0	29	20
Siebenquell	−10.0	26	20

Table 4
Average chemical compositions, temperatures, field pH and electrical conductivities (EC) of analyzed ground- and thermal water based on samples from the GFZ field survey conducted in 2022–2024. Individual measurements available in Prause et al. (2026).

Location	T (°C)	pH	EC (mS·cm^{-1})	HCO_3^- (mg·L^{-1})	Cl^- (mg·L^{-1})	F^- (mg·L^{-1})	Br^- (mg·L^{-1})	NO_3^- (mg L^{-1})	SO_4^{2-} (mg·L^{-1})	Na^+ (mg·L^{-1})	K^+ (mg·L^{-1})	Li^+ (mg·L^{-1})	Ca^{2+} (mg·L^{-1})	Mg^{2+} (mg·L^{-1})	Sr^{2+} (mg·L^{-1})	Fe_{tot} (mg·L^{-1})	SiO_2 (mg·L^{-1})	TDS[a] (mg·L^{-1})	CBE[b] (%)
Thermal Water:																			
Neumühle	22.9	7.5	10.36	33	3349	2.3	21	0.2	211	797	9.8	2.1	1274	15	16	1.3	21	5755	0.3
Schönbrunn (453 m)[c]	33.6	7.4	3.8	75	1135	6.1	6.5	n.a.	240	681	8.3	1	180	6.4	5.8	0.17	24	2410	1.2
Warmbad	25	7.3	0.495	159	47	3.9	0.13	19	29	70	4.3	<1	26	4.3	0.26	0.03	26	389	−2.4
Georgsquelle	23.9	7.2	0.605	318	26	5.5	<0.1	2	13	116	5.3	<1	12	2	0.12	0.03	39	539	−4.7
Siebenquell	31.9[d]	8.3	0.425	92	60	6.9	0.42	<0.1	31	65	≤2.5	<1	19	0.09	0.17	≤0.14	34	309–311	~−5[e]
Groundwater:																			
Geilsdorf Deep Well	11.5	7.3	0.454	189	23	0.28	<0.1	<0.1	46	13	<1	<1	61	13	0.27	0.09	17	362	−0.4
Wiesenbad Groundwater Well	18.4	7	0.514	165	58	3.3	0.1	4.7	22	75	6.1	<1	20	3.7	0.16	1.6	32	394	−3.3
Radonquelle Weißenstadt	9.6	5.8	0.1	15	13	0.3	<0.1	0.29	11	10	1.3	<1	6.1	1.8	0.05	0.05	28	88	3.4
Brüder Einigkeit Mine Tunnel	13.7	7.7	1.489	248	229	3.5	≤1.2	<1.1	185	173	4.3	<1	108	23	1.2	0.09	10	987	1.3

[a] Total Dissolved Solids (inorganic only).
[b] Charge Balance Error = (∑cations-∑anions)/(∑cations+∑anions)•100%, where concentrations are in meq·L^{-1}.
[c] Composition of the Schönbrunn (453 m) thermal water based on measurements from 1994 to 1996 obtained as part of DFG-Projects Nr. Str 376/2, Nr. Ka 902/3 (Prause et al., 2026).
[d] Cooled down from ~53 °C prior to sampling.
[e] Between −5.3 and −4.5, reflecting variable K concentrations of 0–2.5 mg·L^{-1} (see Prause et al., 2026).

$\delta^{18}O$ of −13.9 to −3.9 ‰ SMOW and δ^2H of −103.8 to −24.5 ‰ SMOW (Fig. 4a), plotting close to both the Global Meteoric Water Line (GMWL) (Craig, 1961):

$$\delta^2H = 8 \times \delta^{18}O + 10 \quad (6)$$

and the Local Meteoric Water Line (LMWL) for Germany (Stumpp et al., 2014):

$$\delta^2H = 7.72 \times \delta^{18}O + 4.9 \quad (7)$$

Stable isotope ratios of non-thermal groundwater and thermal water fell within the same range as those of the surface water (Fig. 4b) but showed less variation, with $\delta^{18}O$ of −10.1 to −9.8 ‰ SMOW and δ^2H of −75.6 to −65.9 ‰ SMOW. Tritium contents of non-thermal groundwater were slightly lower than those of surface water, ranging between 1.6 to 3.1 TU. By contrast, tritium contents of most thermal water were much lower and below detection limits in most cases, the only exception being the Warmbad thermal water, in which tritium contents ranged between 2.2 to 2.5 TU.

4.3. Geothermometry

4.3.1. Empirical geothermometers

Results of empirical geothermometers for individual thermal waters analyzed in this study are summarized in Table 6 and Fig. 5. All geothermometers except for the Na-K geothermometer indicated temperatures of < 100 °C for the studied locations. Estimated temperatures for the same location were found to show significant variations between the four Na-K geothermometers.

The conditions for applying an Mg correction to the Na-K-Ca geothermometer were not fulfilled, either because calculated temperatures were < 70 °C or because the calculated correction value of ΔT_{Mg} was negative for thermal water with $R = Mg_{meq/L}/(Mg_{meq/L}+Ca_{meq/L}+K_{meq/L}) < 50$ (Fournier and Potter, 1979). Hence, all results of the Na-K-Ca geothermometer are reported without an Mg correction. A comprehensive review of the Mg correction procedure and the conditions for its use are beyond the scope of this paper and the reader is instead referred to Fournier and Potter (1979) for further details.

4.3.2. Multicomponent equilibrium geothermometry

According to MEG modeling the thermal water at Neumühle equilibrated with an assemblage of kaolinite, calcite, quartz, muscovite and montmorillonite at a temperature of ~61 °C and underwent minor degassing of 0.085 mmol CO_2·kgw^{-1} with little to no dilution by shallow groundwater (Fig. 6a). The modeled equilibrium mineral assemblage of the Schönbrunn (453 m) thermal water was identical to the one at Neumühle. Modeled reservoir temperatures at Schönbrunn were ~83 °C, applying a dilution factor of 1.5 and accounting for degassing of 0.7 mmol CO_2·kgw^{-1} (Fig. 6b). At Warmbad and Georgsquelle, MEG modeling suggested equilibration of both thermal waters with a mineral assemblage consisting of kaolinite, quartz, calcite, saponite and clinochlore at temperatures of ~74 °C and ~86 °C, respectively, and no significant degassing of CO_2 or dilution with groundwater (Fig. 6c and d). At Siebenquell, a high dilution factor of 1.75, high extents of CO_2 degassing of 1.5 mmol CO_2·kgw^{-1} and an additional correction of Mg activities by equilibration with clinochlore-14 Å had to be included in the model in order to find a feasible solution. Two equilibrium temperatures were derived for the Siebenquell thermal water: ~85 °C, assuming equilibration with chalcedony, kaolinite, clinochlore and saponite and ~107 °C, assuming equilibration with quartz, calcite, kaolinite and clinochlore.

4.3.3. Silica enthalpy mixing models

Temperatures estimated by the silica enthalpy mixing model were generally higher than those derived from most of the empirical geothermometers and MEG modeling. For Neumühle, the silica enthalpy

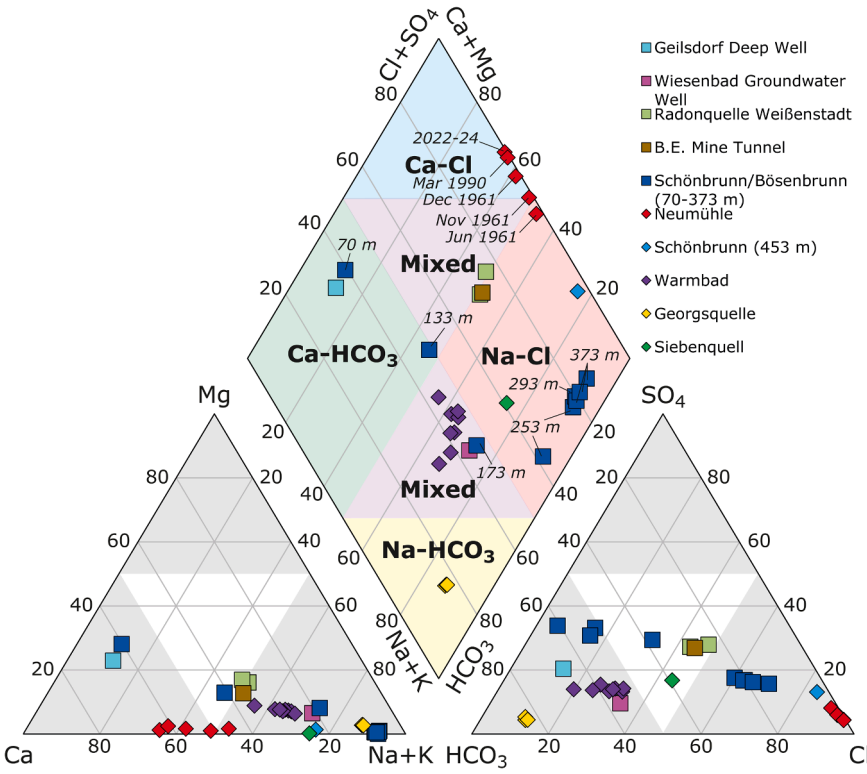

Fig. 2. Piper diagram showing the compositions of samples included in this study. Diamond and square symbols indicate thermal water and non-thermal groundwater, respectively. Relative abundances of anions and cations are in meq·L^{-1}. Data from: Prause et al. (2026).

mixing model predicted a reservoir temperature of ~100 °C, and, assuming mixing with non-thermal groundwater from the Geilsdorf Deep Well, a fraction the deep hot water component F_{HW} of 0.13 (Fig. 7a). For the Schönbrunn (453 m) thermal water, mixing was assumed with mine water from the Brüder Einigkeit Mine Tunnel, yielding temperatures of 133 °C and a fraction of F_{HW} of 0.17 (Fig. 7b). The Georgsquelle thermal water was the only thermal water for which predicted temperatures were high enough to include an estimate assuming steam loss (Eq. (3)). If mixing with water from the Wiesenbad Groundwater Well and steam loss were assumed, the estimated temperature of the hot water component at Georgsquelle was estimated as 147 °C and the corresponding F_{HW} was 0.07 (Fig. 7c). Assuming no steam loss, the estimated temperature of the hot water component was 195 °C and F_{HW} was 0.03 (Fig. 7c). Assuming mixing between the Siebenquell thermal water and the non-thermal groundwater from the nearby Radonquelle spring, F_{HW} at Siebenquell was 0.23 and the temperature of the hot water component was estimated as 105 °C (Fig. 7d). For Warmbad, no corresponding local groundwater to serve as a potential cold endmember was available. Since silica concentrations measured at the Wiesenbad Groundwater Well were higher than the ones in the Warmbad warm spring (Table 4), the silica enthalpy mixing model could not be applied to these two waters.

4.4. Circulation depths and recharge elevations

Unless specified otherwise, temperatures predicted by MEG modeling (Fig. 6), which included corrections for dilution and CO_2 degassing and which were generally compatible with results of the empirical geothermometers, were used as values for T_{res} in Eq. (4). The thermal waters of Neumühle and Schönbrunn (453 m) from the SW-Vogtland region had similar recharge elevations h_R of 843–868 MASL (meters above sealevel) (Table 7). The circulation depth of the Neumühle thermal water was estimated to be ~1.8 km and thus significantly shallower than that of the Schönbrunn (453 m) thermal water of ~2.6 km. Recharge elevation of the thermal waters of Warmbad and Georgsquelle from the Central Erzgebirge region were nearly identical at ~757 MASL and ~758 MASL, respectively, and the waters were estimated to have circulated to comparable depths of ~2.3 and ~2.7 km, respectively (Table 7). For the Siebenquell thermal water, two circulation depths were estimated based on a low temperature estimate of ~54 °C according to the chalcedony geothermometer (Table 6) and a higher estimate assuming a temperature of ~107 °C, compatible with both the results of the silica enthalpy mixing model and the maximum temperature predicted by MEG modeling (Figs. 6e and 7d). The shallow estimate for the Siebenquell thermal water was ~1.8 km, equal to the depth of the Siebenquell borehole (Röckel and Stober, 2017), whereas the deep estimate was ~3.8 km (Table 7). The estimated recharge elevation of the Siebenquell thermal water was ~754 MASL.

5. Discussion

5.1. Reservoir temperatures

Among the empirical geothermometers, temperatures of < 100 °C are predicted for each of the studied thermal waters by all but the Na-K geothermometers, which in some cases indicated higher temperatures. Furthermore, significant scattering was observed between the results of individual Na-K geothermometers (Table 6, Fig. 5). The various Na-K geothermometers are based on temperature sensitive cation exchange reactions involving Na and K occurring between albite and orthoclase (Fournier, 1979; Fournier and Truesdell, 1970). Because cation exchange slows down considerably at lower temperatures and dissolved Na and K concentrations tend to be more strongly controlled by clay minerals rather than feldspars under such conditions, the Na-K geothermometer generally works best for reservoir temperatures of 180–350 °C, but may deliver inaccurate results outside of this temperature range (Ellis, 1970, 1979; Giggenbach, 1988; Li et al., 2020; Nicholson, 1993). Conversely, the slow re-equilibration of the Na-K

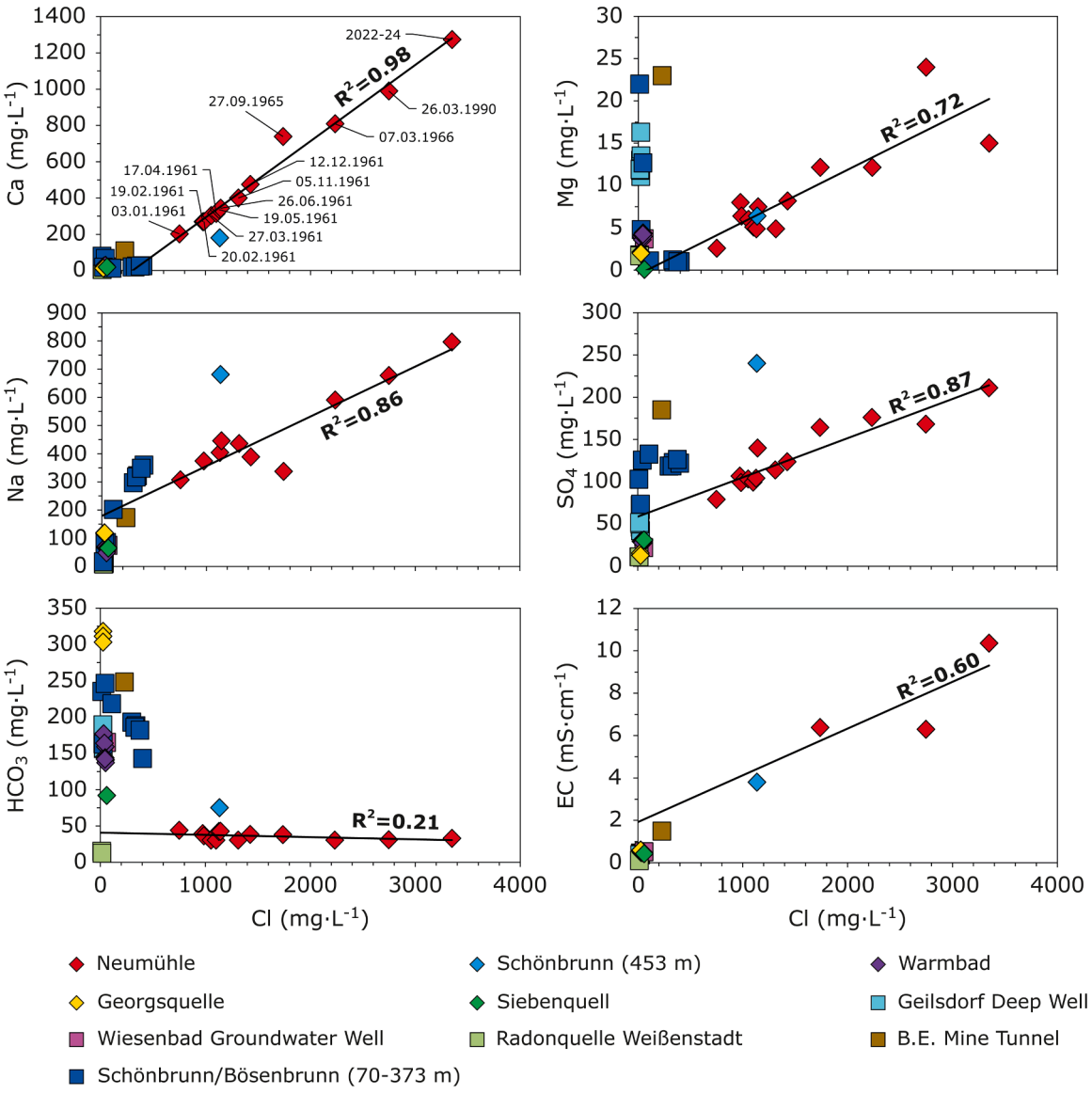

Fig. 3. Chloride vs element plots for groundwater (squares) and thermal water (diamonds). Composition of the Neumühle thermal water has shifted between 1961 and 2024 towards higher Cl, Ca, Mg, Na, SO_4 and electrical conductivity (EC) while HCO_3 has remained unaffected by this development. Data from: Prause et al. (2026).

geothermometer also allows it to retain information of the deep reservoir, which can be lost due to the rapid re-equilibration of other geothermometers (Nicholson, 1993; Simmons, 2013). This means that the higher temperatures predicted by the Na-K geothermometers could be either due to preservation of deep fluid-mineral equilibria not recorded by the other empirical geothermometers or because reservoir conditions were unsuitable for the application of a Na-K geothermometer. The latter interpretation is considered more likely in this case, due to 1) the high scattering between individual Na-K geothermometers, 2) all thermal water having ratios for the molal concentrations of $\sqrt{m_{Ca}}/m_{Na}$ much higher than the proposed threshold value of unity for the applicability of the Na-K geothermometer (Fournier and Truesdell, 1973) and 3) estimated temperatures by the Na-K geothermometers being generally below the recommended range of applicability of 180–350 °C for all locations. A general failure of the Na-K and K-Mg geothermometer to attain simultaneous equilibrium is also indicated by the Na-K-Mg ternary diagram after Giggenbach (1988) (Fig. 8a), which indicated only partial equilibrium for the thermal waters at Neumühle and Schönbrunn, while the thermal waters at Warmbad and Georgsquelle were identified as “immature waters”, further highlighting that the results of the slowly-equilibrating Na-K geothermometer need to be considered critically. Thus, it is suggested that the Na-K geothermometer likely did not produce accurate results for the thermal waters investigated in this study.

The K-Mg geothermometer (Giggenbach, 1988), which is based on the relative stabilities of muscovite and clinochlore versus alkali feldspars at variable temperature, equilibrates much faster than the Na-K geothermometer at lower temperatures and generally is most accurate at temperatures < 150 °C (Li et al., 2020; Nicholson, 1993). Therefore, even though Fig. 8A suggests no simultaneous equilibration of the Na-K and K-Mg geothermometers, the K-Mg geothermometer may still deliver reliable results, assuming that fluid-mineral equilibria involving K and Mg in the reservoir are primarily controlled by the reactions outlined above and no significant modification of the ionic ratios of K^+ and Mg^{2+}, e.g., due to mixing with shallower groundwater, boiling or re-equilibration, has occurred (Li et al., 2020; Nicholson, 1993).

Like the K-Mg geothermometer, the silica geothermometer equilibrates relatively quickly even at low temperatures and is known to

Table 5
Ranges of stable isotope ratios of water ($\delta^{18}O$ and $\delta^{2}H$) and tritium (^{3}H) contents of analyzed ground-, thermal and surface water. Individual measurements available in Prause et al. (2026).

Location	$\delta^{18}O$ (‰ SMOW)	$\delta^{2}H$ (‰ SMOW)	^{3}H (TU)[a]
Thermal Water:			
Neumühle	−10.5 to −10.3	−70.9 to −69.7	< 1.0
Schönbrunn (453 m)	−10.7 to −10.3	−75.6 to −72.8	≤ 1.2
Warmbad	−10.2 to −9.9	−67.5 to −66.1	2.2 to 2.5
Georgsquelle	−10.1 to −9.9	−68.0 to −65.9	≤ 1.0
Siebenquell	−10.1 to −9.8	−67.9 to −66.3	≤ 1.1
Groundwater:			
Geilsdorf Deep Well	−10.0 to −9.9	−69.6 to −67.8	1.6 to 2.1
Brüder Einigkeit Mine Tunnel	−10.1 to −9.8	−69.5 to −68.0	2.6 to 3.1
Surface Water:			
Hof (Rainwater) – DWD 2022	−13.9 to −3.9	−103.8 to −24.5	4.2 to 13.7
Geilsdorf (Rainwater)	−7.4 to −4.9	−46.6 to −32.4	8.1 to 11.0
Kemnitzbach (River Water)	−9.3 to −8.8	−64.0 to −61.8	2.2 to 7.3

[a] Values from 2022–2024.

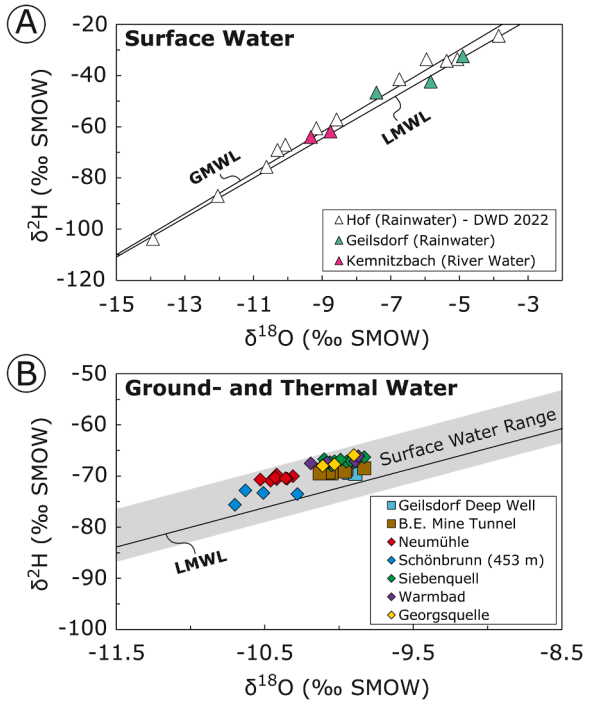

Fig. 4. Stable oxygen and hydrogen isotope ratios ($\delta^{18}O$ and $\delta^{2}H$) of surface water (triangles), groundwater (squares) and thermal water (diamonds) included in this study. A) Range of isotopic ratios of surface water including rainwater from 2022 from the local DWD weather station in the town of Hof, sampled as part of the German Isotope Network (Schmidt et al., 2020 Koeniger et al., in prep.). All surface water plotted close to both the Global Meteoric Water Line (GMWL, Craig, 1961) and the Local Meteoric Water Line for Germany (LMWL, Stumpp et al., 2014). B) Range of stable oxygen and hydrogen isotope ratios of ground- and thermal water. Grey shaded area shows the range of isotope ratios of surface water plotted in part A of the figure. All ground- and thermal water plotted within the same range as local surface water. Data from: Prause et al. (2026).

deliver reliable results at temperatures < 250 °C, assuming no modification of aqueous silica concentration by water-rock interaction, boiling, dilution or mixing with shallow groundwater between the geothermal reservoir and the surface (Fournier, 1985; Nicholson, 1993). Furthermore, the selection of the correct SiO_2 polymorph controlling silica solubility in the reservoir is crucial for the precise determination of temperatures with this type of geothermometer. The activity of aqueous silica is generally more likely to be controlled by chalcedony rather than quartz at temperatures < 90–140 °C, especially in systems where the availability of silica is low and pH reaches alkaline values, as is the case in many well-studied Icelandic geothermal systems, typically hosted in basaltic lithologies (Arnórsson, 1975; Fournier, 1985). However, as noted by Arnórsson et al. (1983), the attainment of quartz equilibrium is observed in several low-temperature geothermal systems outside of Iceland. This observation is corroborated by the results of several studies in both granitic and non-granitic geothermal systems, which indicated that the equilibration of quartz below 100 °C is possible (Blasco et al., 2017; Simmons, 2013; Zhao et al., 2023). In fact, the exact nature of the silica polymorph controlling $SiO_{2,aq}$ activity is not a simple function of temperature and quartz may well achieve stability at low temperatures in relatively saline solutions, particularly if the availability of silica is high and pH is about neutral or if residence times are sufficiently long for significant water-rock interaction to take place (Arnórsson, 1975; Arnórsson et al., 1983; Fournier, 1985; Morey et al., 1962). It is thus helpful to consider geochemical signatures serving as proxies for the extent of water-rock interaction when selecting a suitable silica geothermometer. Chloride is often actively and passively enriched over the course of water-rock interaction in deep aquifers and geothermal systems due to 1) dissolution of halite and admixture of saline brines, 2) introduction of HCl from underlying magmatic bodies and 3) the removal of HCO_3 and SO_4 as carbonates, e.g., calcite, and sulfates, e.g., anhydrite, precipitate during the heating of the recharging water because of their retrograde solubilities (Alçiçek et al., 2018; Giggenbach, 1988; Han et al., 2010; Hardie, 1990; Lowenstein and Risacher, 2009; Michard, 1990). Chloride enrichment at depth is then typically preserved as the thermal water cools and rises to the surface, because Cl usually maintains near full mobility and does not take part in any mineral formation reactions in most cases. The thermal waters from the SW-Vogtland region, Neumühle and Schönbrunn (453 m), are both highly evolved “mature” Cl-rich waters (Fig. 8b) and are both highly mineralized based on measured TDS and EC while exhibiting low tritium contents of ≤ 1.2 TU, indicating extensive water-rock interaction (Fig. 8c). While mineralization of the Georgsquelle, Siebenquell and Warmbad thermal waters was an order of magnitude lower than for Neumühle and Schönbrunn (453 m), both Georgsquelle and Siebenquell had comparably low tritium contents of ≤ 1.1 TU, likewise suggesting prolonged circulation (Fig. 8c). A comparison of the predicted temperatures using various different silica geothermometers with those of the similarly quickly equilibrating K-Mg geothermometer (Giggenbach and Goguel, 1989) is shown in Fig. 8d In this diagram, each of the plotted curves signifies a range of water compositions where the temperatures predicted by the K-Mg geothermometer fully agree with those of the silica geothermometers of quartz, chalcedony, α- and β-cristobalite and amorphous silica. Plotting the composition of thermal water analyzed in this study in this diagram indicates that silica solubility is likely controlled by quartz at Neumühle and Schönbrunn and either by quartz or chalcedony at Georgsquelle. The stability of quartz in the Georgsquelle geothermal system is supported by the presence of hydrothermal quartz mineralization in the Wiesenbad fault zone along which the Georgsquelle thermal water ascends to the surface (Kuschka, 1997, 2002; von Storch et al., 2000). Although tritium contents of the Warmbad thermal water were higher than for the other thermal waters (Fig. 8c), Fig. 8d suggests that silica solubility may also alternatively be controlled by chalcedony or quartz for this location. As mentioned above, K concentrations of the Siebenquell thermal water could not be constrained with sufficient confidence and thus Siebenquell was omitted in Fig. 5d Varying K concentrations in a range of <1 but >0 $mg{\cdot}L^{-1}$ indicated silica solubility at Siebenquell to be controlled by chalcedony, whereas assuming the maximum measured K concentration of 2.5 $mg{\cdot}L^{-1}$ indicated silica solubility being controlled by quartz.

Unlike the Na-K and K-Mg geothermometers, the empirical geothermometers for the systems Na-K-Ca (Fournier and Truesdell, 1973)

Table 6
Summarized results of empirical geothermometry. With the exception of the results for Schönbrunn (453 m), calculations are based on measurements from the 2022–2024 GFZ field survey (Prause et al., 2026). The results for Schönbrunn (453 m) are based on fluid compositions measured in 1994 to 1996 as part of DFG-Projects Nr. Str 376/2 and Nr. Ka 902/3 (Prause et al., 2026). No geothermometers involving K concentrations were applied to the Siebenquell thermal water, because K was not unambiguously constrained (see 4.1). Uncertainties ($\pm x$) are reported as two standard deviations of n measurements.

Geothermometers	Neumühle		Schönbrunn (453 m)		Warmbad		Georgsquelle		Siebenquell	
	T_{calc} (°C)	n	T_{calc} (°C)	n	T_{calc} (°C)	n	T_{calc} (°C)	n	T_{calc} (°C)	n
Na-K (Santoyo and Diaz-Gonzales, 2010)	41 ± 8	20	41 ± 15	97	146 ± 31	3	122 ± 4	3	-	-
Na-K (Fournier, 1979)	86 ± 7	20	85 ± 14	97	178 ± 26	3	158 ± 4	3	-	-
Na-K (Giggenbach, 1988)	107 ± 7	20	106 ± 14	97	196 ± 25	3	177 ± 3	3	-	-
Na-K (Arnórsson and Gunnlaugsson, 1983)	48 ± 7	20	48 ± 15	97	150 ± 30	3	127 ± 4	3	-	-
Na-K-Ca (Fournier and Truesdell, 1973)	36 ± 3	20	66 ± 8	97	62 ± 6	3	91 ± 3	3	-	-
Na-K-Ca-Mg (Nieva and Nieva, 1986)	57 ± 3	20	90 ± 9	97	27 ± 2	3	34 ± 1	3	-	-
K-Mg (Giggenbach, 1988)	61 ± 3	20	67 ± 6	97	57 ± 6	3	70 ± 1	3	-	-
Quartz, conductive (Fournier, 1977)	65 ± 4	20	70 ± 5	46	74 ± 0	3	91 ± 4	3	85 ± 0	2
Quartz, adiabatic (Fournier, 1977)	71 ± 3	20	75 ± 5	46	78 ± 0	3	93 ± 3	3	88 ± 0	2
Chalcedony, conductive (Fournier, 1977)	33 ± 4	20	39 ± 5	46	42 ± 0	3	60 ± 4	3	54 ± 0	2

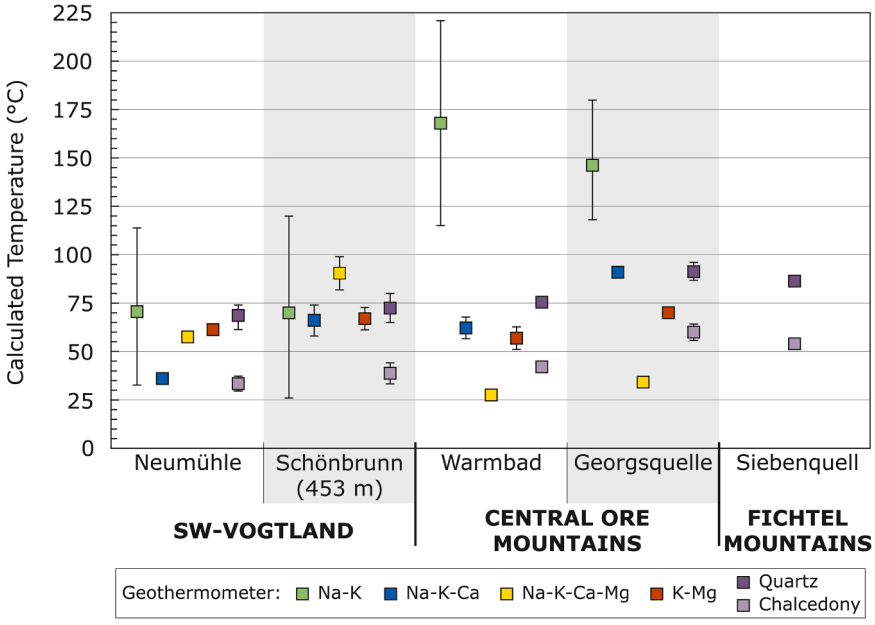

Fig. 5. Results of different empirical geothermometers for thermal waters included in this study. Due to temperatures predicted by silica geothermometry being < 100 °C for all thermal waters, only results from the conductive quartz and chalcedony geothermometers are shown. Error bars indicate two standard deviations of n measurements (see Table 6).

and Na-K-Ca-Mg (Nieva and Nieva, 1987) are not tied to a specific equilibrium mineral assemblage but are calibrated based on large chemical datasets of fluids of known composition and temperature. Thus, their advantage lies in incorporating a much broader range of possible water-rock reactions. The inclusion of Ca, however, may present a problem in some cases, because this element is strongly linked to the carbonate system and therefore any geothermometer relying on Ca concentrations may be susceptible to variable pCO_2 (and therefore pH) as well as carbonate dissolution or precipitation, especially at low temperatures (Arnórsson et al., 1983; Giggenbach, 1988). Although the inclusion of Mg in the Na-K-Ca-Mg geothermometer and the application of a correction for Mg contents published for the Na-K-Ca geothermometer (Fournier and Potter, 1979) partially mitigates this problem, the application of these geothermometers to bicarbonate water and lower temperature (< 180 °C) systems may in some cases lead to inaccurate results (Arnórsson et al., 1983; Li et al., 2020; Nicholson, 1993; Pope et al., 1987).

Reservoir temperatures predicted by MEG fell within the same range as those derived from empirical geothermometry (compare Figs. 5 and 6). Moreover, estimated dilution factors from MEG modeling may provide important insights into the validity of the assumption of mixing with shallow groundwater required by the silica enthalpy mixing model: No dilution was required in order for saturation indices to converge on a feasible solution for the thermal waters at Neumühle, Georgsquelle and Warmbad. This may suggest that these waters are relatively undilute and have experienced little to no mixing with shallow groundwater along their flowpath to the surface. Results of the silica enthalpy mixing model for the thermal waters at Neumühle and Georgsquelle (Figs. 7a and c) were therefore not included in the estimated range of reservoir temperatures. In the case of the Schönbrunn (453 m) thermal water, the temperature of 133 °C estimated by assuming mixing with water from the Brüder Einigkeit Mine Tunnel (Fig. 7b) far exceeded the range defined by the results of the empirical geothermometers and MEG modeling (Figs. 5 and 6). The Brüder Einigkeit Mine Tunnel water also contained between 2.6 to 3.1 TU tritium, whereas the Schönbrunn (453 m) thermal had tritium contents of ≤ 1.2 TU (Table 5). Therefore, it can be ruled out that the Schönbrunn (453 m) thermal water is a mixture containing ~83 vol.% of the Brüder Einigkeit Mine Tunnel water as suggested by the silica enthalpy mixing model (Fig. 7b). Moreover, mixing calculations (supplementary material S.2) revealed that the

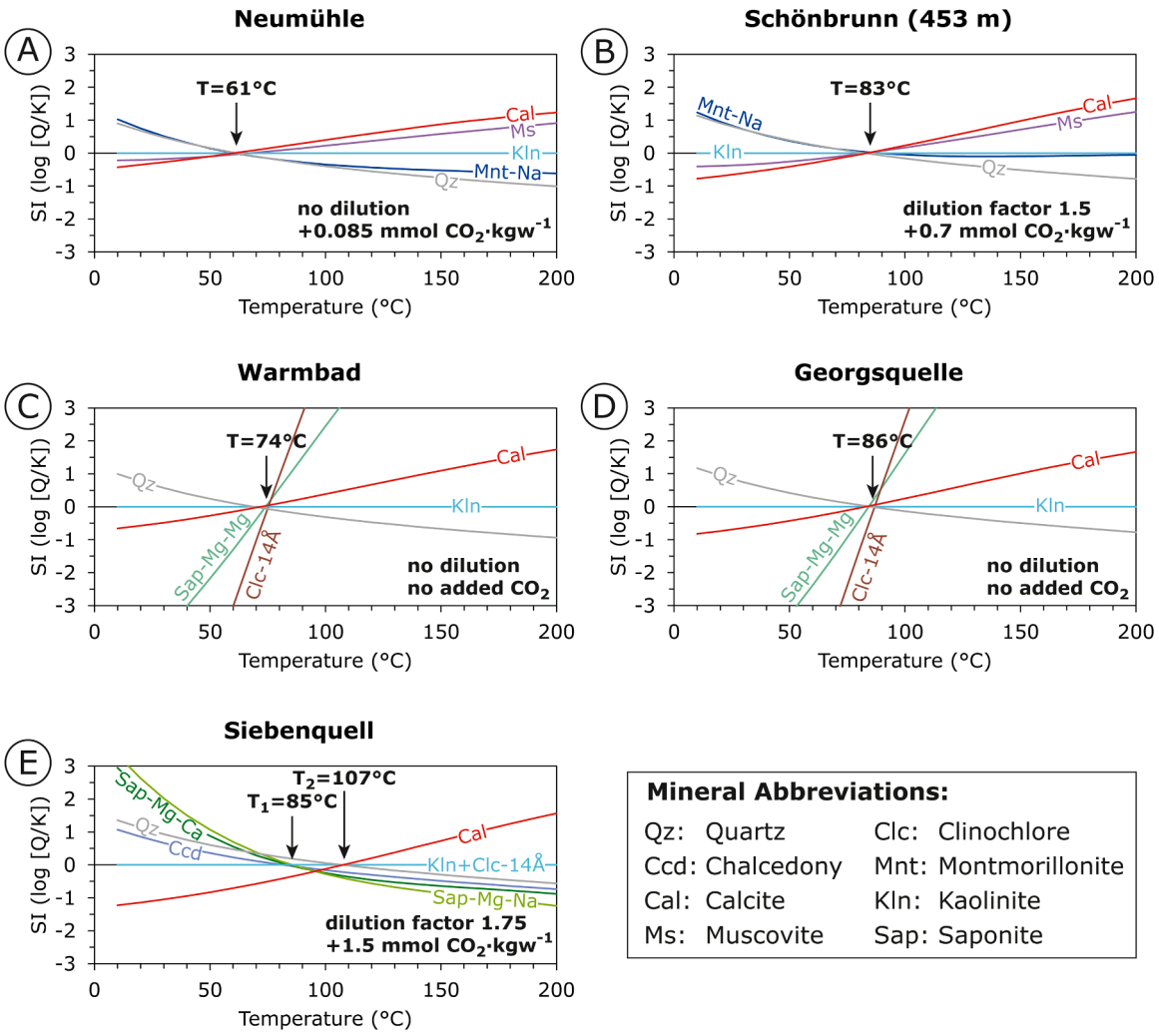

Fig. 6. Results of multicomponent equilibrium geothermometry derived for thermal water from A) Neumühle, B) Schönbrunn, C) Warmbad, D) Georgsquelle and E) Siebenquell. Equilibrium with kaolinite (Kln) was assumed to account for missing Al activities. In the case of Siebenquell, an additional correction of Mg activities was applied by assuming equilibrium with clinochlore (Clc-14 Å).

water from the Brüder Einigkeit Mine Tunnel and the Schönbrunn (453 m) thermal water were unlikely to be related by simple two-component mixing. Hence, although the Schönbrunn (453 m) thermal water may have been diluted by groundwater along its flowpath according to MEG (Fig. 6), it is concluded that the diluting component likely was a deep groundwater with long average residence times and a potentially much different silica concentration and enthalpy compared to the water from the Brüder Einigkeit Mine Tunnel. Thus, the results of the silica enthalpy mixing model for the Schönbrunn (453 m) thermal water were not included in our estimations of reservoir temperatures. At Siebenquell, MEG modeling hinted at extensive dilution and indicated two separate equilibrium mineral parageneses, consisting of kaolinite, clinochlore, chalcedony and saponite at ~85 °C and kaolinite, clinochlore, quartz and calcite at ~107 °C (Fig. 6e). This suggests that the thermal water may have experienced significant mixing and/or re-equilibration on its way to the surface. The higher temperature estimate is compatible with the results of the silica enthalpy mixing model predicting temperatures of ~105 °C. On the other hand, the temperature of ~54 °C predicted for Siebenquell by the chalcedony geothermometer is independently supported by direct temperature measurements at the bottom and top of the Siebenquell borehole of ~53.4 °C and ~53 °C, respectively (Röckel and Stober, 2017). These observations suggest that a fraction of the Siebenquell thermal water may have originated from a deeper hotter reservoir with temperatures of up to 107 °C before mixing with more shallow ground- and thermal water in the Siebenquell borehole followed by re-equilibration of the mixture at a temperature of ~54 °C.

Taking into account the considerations on the applicability of various empirical geothermometers to the individual thermal waters treated in this study as outlined above, ranges for reservoir temperatures of each thermal water were estimated as summarized in Table 8. If the result of a specific geothermometer fell within 20 °C of sampling temperature, the calculated temperature was assumed to be affected by re-equilibration under close-to-surface conditions and not included in the final temperature estimate (e.g., Fournier, 1973, 1981, Giggenbach 1988). This was the case for the chalcedony geothermometer at Neumühle, Schönbrunn and Warmbad, the Na-K-Ca-Mg geothermometer at Wambad and Georgsquelle as well as the Na-K-Ca geothermometer at Neumühle (compare Tables 4 and 6).

5.2. *Recharge areas*

Stable isotope ratios of $\delta^{18}O$ and $\delta^{2}H$ of all thermal water fell within the same range as regional surface water (Fig. 4b), indicating a clear meteoric origin. No signs for the influence of magmatic volatiles, such as H_2S and HCl which may suggest a partially magmatic origin of thermal water was observed (Fig. 8b).

For thermal water sourced from meteoric water, estimations of recharge elevations in the form of Eq. (5) are commonly used in

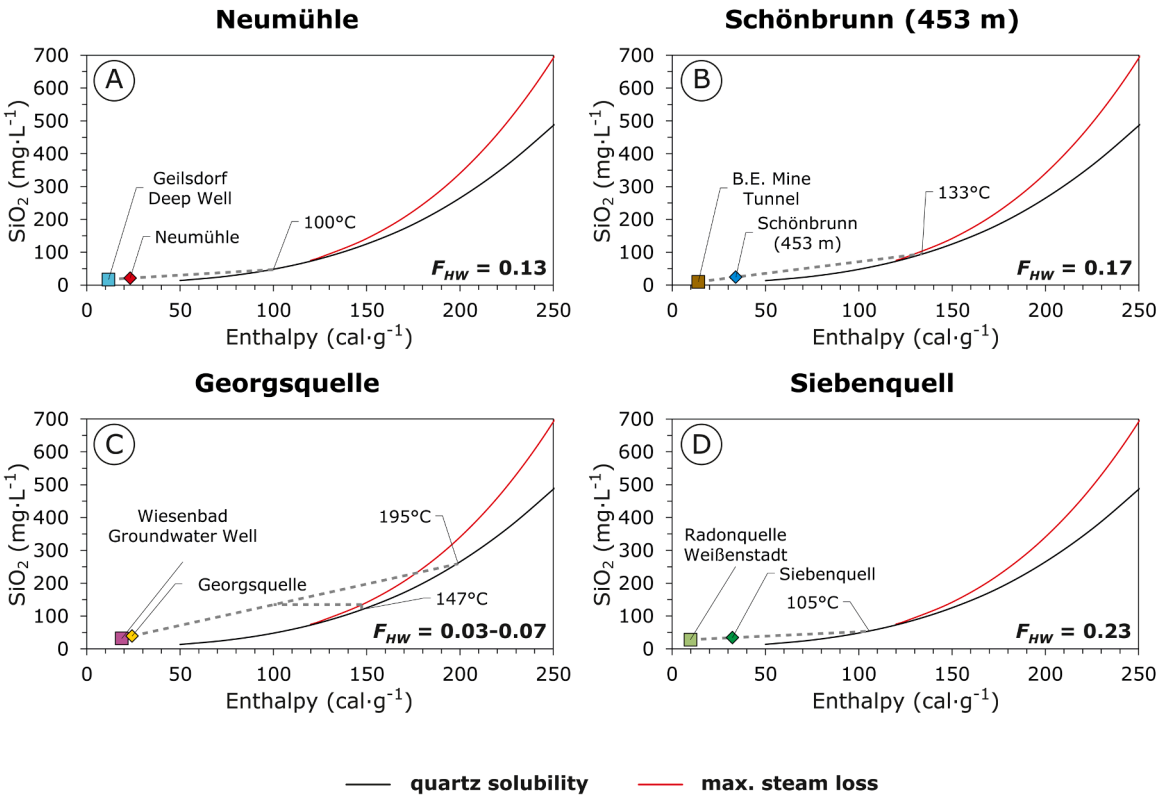

Fig. 7. Results of the silica enthalpy mixing model for A) Neumühle, B) Schönbrunn, C) Georgsquelle and D) Siebenquell. The value of F_{HW} refers to the estimated decimal volume fraction of hot water in mixed thermal water.

Table 7
Recharge elevations (h_R) and circulation depths (d_C) estimated for thermal water included in this study.

Location	h_R (m above sea level)	d_C (km below surface)
Neumühle	843	1.8
Schönbrunn (453 m)	868	2.6
Warmbad	757	2.3
Georgsquelle	758	2.7
Siebenquell (shallow)	754	1.8[a]
Siebenquell (deep)	754	3.8[b]

[a] Shallow estimate, based on a reservoir temperature of 54 °C according to the chalcedony geothermometer.
[b] Deep estimate, based on a maximum temperature of 107 °C according to multicomponent equilibrium geothermometry and the silica enthalpy mixing model.

geochemical surveys (e.g., Mao et al., 2021; Marques et al., 2003; Wang, L. et al., 2023; Xiao et al., 2018). Such estimates are appropriate for early-stage geochemical surveys where detailed data is generally unavailable. In the case of this study, all estimates are based on the composition of thermal water that has been sampled at or near the spring, without detailed information on reservoir conditions in several km depth. Values for $\delta^{18}O_{sw}$ are subject to both short-term inter-annual variations as well as long-term climatic effects, which may influence the estimated recharge elevation according to Eq. (5), particularly if a system contains significant fractions of water that recharged during the last few thousands to tens of thousands of years (Waltgenbach et al., 2021; Weisser et al., 2024; Winter et al., 2024). Furthermore, the studied systems likely recharged over a range of elevations, rather than originating from only one point of recharge at a single well-defined elevation. Mixing with meteoric water from lower altitudes would modify $\delta^{18}O_{tw}$ signatures of the thermal water towards less negative values, potentially leading to an underestimation of the maximum recharge elevation. For these reasons, all recharge elevations derived in the form of Eq. (5) should explicitly be treated as first-order estimates, primarily aimed at constraining main recharge areas.

Estimated recharge elevations for Neumühle and Schönbrunn (453 m) ranged between 843 and 868 MASL (Table 7), indicating a common recharge area. The closest topographic elevation of sufficient height is Aschberg mountain near Klingenthal to the east of both Neumühle and Schönbrunn (50.390°N, 12.509°E) rising to a height of ~936 MASL (Fig. 9a).

At Warmbad and Georgsquelle, estimated recharge elevations were ~757–758 MASL, placing their most likely recharge area in the nearby Ore Mountains (Fig. 9b). The Georgsquelle warm spring is located on the NW-SE striking Wiesenbad fault, whereas the Warmbad warm spring is located on the Marienberg block of the NW-SE striking Neugeboren-Kindlein fault, belonging to the larger Warmbad-Chomutov fault system. The plateau of the Marienberg block reaches up to the top of the Ore Mountains near Kühnhaide-Reitzenhain (50.561°N, 13.219°E) and the basalt dome Hirtstein (50.536°N, 13.193°E) with altitudes from 700–840 MASL. The recharge area of the Wiesenbad fault is flanked southwest by the basalt domes Pöhlberg (50.574°N, 13.031°E) and Bärenstein (50.508°N, 13.019°E) and reaches up to the Satzung-Hirtstein area at an altitude of 840–850 MASL. These elevations are compatible with the estimated recharge elevations, suggesting that the respective geothermal reservoirs were likely recharged by water migrating along these two fault systems.

At Siebenquell, the estimated recharge elevation was ~754 MASL, identifying the 877 m high granite plateau of Großer Waldstein (50.129°N, 11.855°E), located 3–4 km northwest of Weißenstadt as the closest recharge area for this system. Further likely recharge areas of the Siebenquell system include the Schneeberg (50.052°N, 11.854°E) and Ochsenkopf (50.031°N, 11.809°E) mountains to the south/southwest (Fig. 9c).

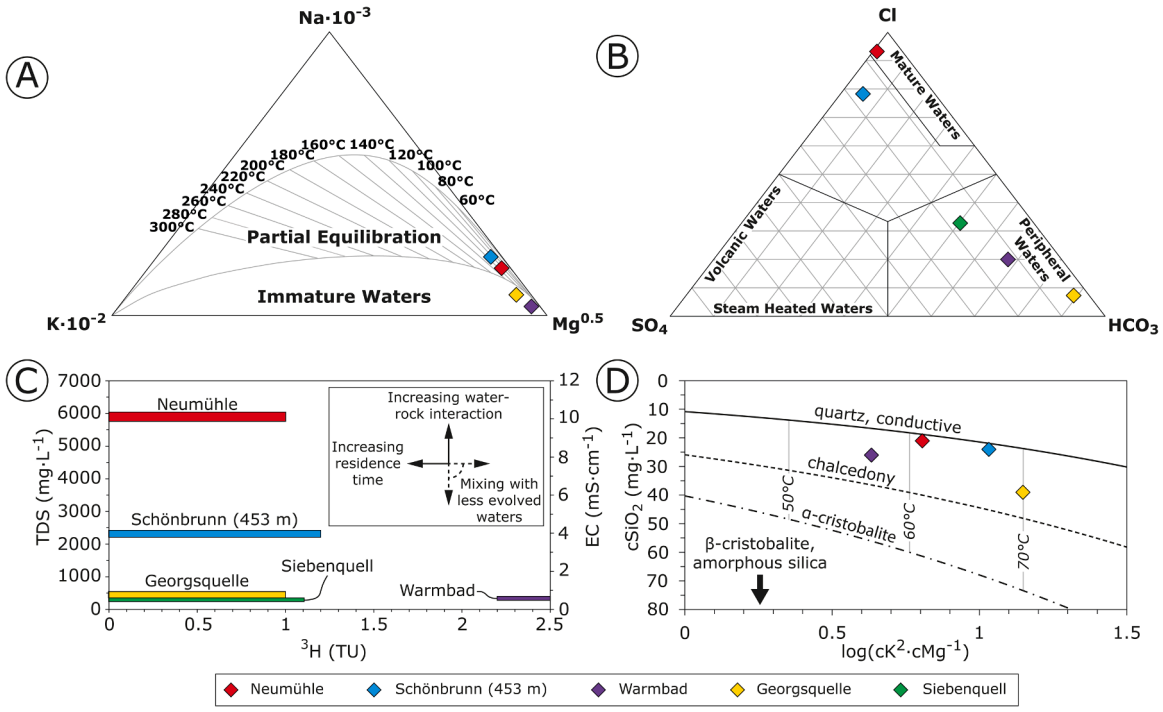

Fig. 8. Summary of equilibration and relative extent of water-rock interaction of studied thermal water. A) Na-K-Mg ternary diagram (Giggenbach, 1988). The thermal waters at Warmbad and Georgsquelle plot within the field of immature waters, indicating low extent of water-rock interaction or potential mixing with shallow groundwater, whereas the Neumühle and Schönbrunn (453 m) thermal waters are partially equilibrated, indicating relatively more extensive chemical exchange with host rock in their respective reservoirs. B) Cl-SO_4-HCO_3 ternary diagram (Giggenbach, 1991). Thermal waters from Siebenquell, Warmbad and Georgsquelle are high in HCO_3, low to intermediate in Cl and low in SO_4, indicating peripheral waters, reflecting either low degrees of water-rock interaction, external CO_2 input, or extensive mixing of thermal water and non-thermal groundwater. By comparison, the Neumühle and Schönbrunn (453 m) thermal waters are Cl-rich "mature" waters that have undergone higher extents of water-rock interaction, supporting the results of the Na-K-Mg ternary diagram. None of the thermal waters plotted near the fields for steam heated or volcanic waters, which indicates a general absence of the influence of H_2S-rich vapors and H_2S-HCl-bearing magmatic fluids as may frequently be observed in volcanically active regions. C) Ranges of tritium contents (TU) as indicator of average residence time vs total dissolved solids (TDS) and electrical conductivity (EC) as indicators of mineralization and water-rock interaction for analyzed ground- and thermal water. Tritium contents refer to recent (2022–2024) values for all locations except for Schönbrunn (453 m), where no new sampling could be carried out. Hence, tritium contents for Schönbrunn (453 m) refer to values measured between 1992–1994 as reported in Prause et al. (2026). D) Plot of cK^2/cMg vs $cSiO_2$ (Giggenbach and Goguel, 1989). Solid and dashed lines indicate hypothetical fluid compositions for which temperatures predicted by the K-Mg geothermometer and various silica geothermometers are in full agreement. Water compositions suggest that silica solubility is controlled by quartz at Neumühle and Schönbrunn (453 m) and either by quartz or chalcedony at Georgsquelle and Warmbad.

5.3. *Origin and circulation of thermal waters*

Simplified conceptual models of the geothermal systems in the regions of the SW-Vogtland, the Central Ore Mountains and the Fichtel Mountains are synthesized based on the results of this study and currently available models of subsurface geology (Stephan et al., 2015, 2018) (Figs. 10–12). Each conceptual model is discussed in detail below.

5.3.1. *Neumühle and Schönbrunn*

The thermal waters of Neumühle and Schönbrunn (453 m) from the SW-Vogtland likely recharge at Aschberg mountain at elevations of ~843–868 MASL. Both thermal waters are highly evolved, mature Cl-rich waters (Figs. 2 and 8b), which are commonly produced by prolonged water-rock interaction in deep aquifers, as a result of a combination of the removal of HCO_3 and SO_4 from solution through the formation of carbonates and sulfates upon heating and, in some cases, cation exchange, breakdown of halite, plagioclase and pyroxene as well as admixture of deep brines (Chen et al., 2024; Hardie, 1990; Li et al., 2024; Lowenstein and Risacher, 2009; Wang, H. et al., 2023). As a result of their prolonged deep circulation, both waters are highly mineralized and exhibit very low tritium concentrations (Fig. 8c), which were below detection limit in most cases, even for the older Schönbrunn (453 m) legacy data from 1992 to 1994. In concordance with our assessments, high average residence times on the order of several tens of thousands of years have been estimated based on measured ^{14}C concentrations of 5.9–10.5 pmC, for the Schönbrunn (453 m) and Neumühle thermal waters (von Storch, 1998; von Storch et al., 2000). This combination of high average residence times, high Cl and extensive mineralization suggests that the Neumühle and Schönbrunn reservoirs are structurally isolated and receive limited recharge from modern meteoric water. In addition, the high mineralization and particularly high Cl concentrations of the Neumühle and Schönbrunn (453 m) thermal waters may have implications on their utilization for deep geothermal energy, because of potential scaling and corrosion effects on well pipes (Agemar et al., 2014a; Kaya and Hoşhan, 2005; Nogara and Zarrouk, 2018; Xu et al., 2022).

Mineralization of the Neumühle thermal water was about twice as high when compared to the Schönbrunn (453 m) thermal water (Table 4), which is at least partially explained by the Neumühle thermal water being largely undilute, whereas the Schönbrunn (453 m) thermal water shows signs of dilution by groundwater between the reservoir and the warm spring (Figs. 6a and b). Due to the low tritium concentrations in the Schönbrunn (453 m) thermal water and the depth of the warm spring, being located 453 m underground, the diluting component was likely a deep groundwater with a high average residence time.

The composition of the Neumühle thermal water has undergone a systematic development from a Na-Cl type towards a Ca-Cl type between 1961 and 2024 (Fig. 2), which was accompanied by an increase in the concentrations of Cl, Ca, Mg, Na and SO_4, whereas HCO_3 remained largely unaffected by changing fluid compositions (Fig. 3). The high Ca

Table 8
Ranges of reservoir temperatures predicted for studied geothermal systems. For detailed information on how geothermometers were selected for each location see text (5.1).

Location	Geothermometers	Estimated Reservoir Temperatures
Neumühle	Quartz, conductive K-Mg Na-K-Ca-Mg MEG	54–69 °C
Schönbrunn (453 m)	Quartz, conductive K-Mg Na-K-Ca Na-K-Ca-Mg MEG	58–99 °C
Warmbad	Quartz, conductive K-Mg Na-K-Ca MEG	51–74 °C
Georgsquelle	Chalcedony Quartz, conductive K-Mg Na-K-Ca MEG	56–95 °C
Siebenquell (shallow reservoir)	Chalcedony	54 °C[a]
Siebenquell (deep reservoir)	MEG SiO_2 Enthalpy	105–107 °C

[a] Supported by in-situ temperature measurements of 53–53.4 °C (Röckel and Stober, 2017).

concentrations of the Neumühle warm spring have previously been attributed to calcite dissolution at depth (Schützel and Hösel, 1962). Yet, this hypothesis does not explain the simultaneous increase of the concentrations of Mg, Na, SO_4 and Cl and, more importantly, it is contradicted by the absence of any kind of correlation between Ca and HCO_3 in long term chemical trends (Fig. 3). In fact, calculating the saturation index of calcite for the Neumühle thermal water using PHREEQC suggests slight calcite supersaturation (SI ≈ 0.23), reflecting, if anything, conditions more conducive to calcite precipitation rather than dissolution. However, considering the long residence times and isolated reservoir conditions at Neumühle, combined with the fact that thermal water often quickly reaches saturation with respect to calcite in the reservoir (Arnórsson, 1989), the observed supersaturation at the spring does not necessarily imply calcite precipitation either; rather, a slight supersaturation of calcite was more likely caused by minor amounts of CO_2 degassing and associated pH increase upon depressurization of the thermal water on the way to the surface (Cosmo et al., 2022; Palandri and Reed, 2001; Pang and Reed, 1998) as reflected in the MEG model (Fig. 6a). Furthermore, mixing calculations (supplementary material S.2) also indicated that the compositional drift over time observed at Neumühle could not be explained by simple two-component mixing between a deep thermal water and a shallower groundwater. Thus, the most likely explanation for the observed chemical evolution of the Neumühle warm spring is that the continued extraction of thermal water has, over time, allowed highly saline water, which had been extensively affected by water-rock interaction in the deep reservoir, to reach the surface. Because of the likely isolated reservoir and limited recharge at Neumühle, decreasing water-rock ratios in the reservoir due to continued extraction of thermal water may have contributed further to changes in composition and rising mineralization over time.

An estimated circulation depth of ~2.6 km confirms the association of the Schönbrunn (453 m) thermal water with the concealed granite pluton of Eichigt-Schönbrunn the exact boundaries of which currently remain poorly constrained. Although the estimated circulation depth of ~1.8 km for the Neumühle thermal water is much shallower by comparison, MEG modeling suggested that both the Neumühle and Schönbrunn (453 m) thermal waters have equilibrated with the same mineral assemblage consisting of calcite, muscovite, kaolinite, montmorillonite and quartz in their respective reservoirs (Fig. 6a and b), which supports the hypothesis that the reservoir of the Neumühle thermal water is also situated in the Eichigt-Schönbrunn granite or a mineralogically highly similar reservoir rock.

5.3.2. *Warmbad and Georgsquelle*

Both the Warmbad and Georgsquelle thermal waters likely recharge at a topographic elevation of ~758 MASL in the nearby Ore Mountains. The estimated circulation depths at Warmbad and Georgsquelle are ~2.3 and ~2.7 km, respectively, indicating that they interacted with similar lithologies of local igneous and metamorphic felsic rock, i.e., granite and gneiss, which accounts for the identical equilibrium mineral paragenesis of quartz, calcite, kaolinite, saponite and clinochlore of both reservoirs (Fig. 6c and d). The Georgsquelle and Warmbad thermal waters are mostly undiluted by shallow groundwater according to MEG modeling but are less mineralized and less equilibrated compared to the thermal waters of Neumühle and Schönbrunn (453 m) (Fig. 8a), despite having interacted with similar lithologies at comparable temperatures in their respective reservoirs. This suggests comparatively more vigorous recharge and faster turnover rates of the Georgsquelle and Warmbad thermal waters, contrasting with the more isolated reservoirs at Neumühle and Schönbrunn.

Given the absence of dilution at Georgsquelle, the observed combination of moderate mineralization and low tritium contents suggests that the reservoir is mostly recharged by groundwater with a high average residence time. By contrast, the Warmbad thermal water, while overall similar to the Georgsquelle thermal water in terms of composition, was slightly less mineralized and its tritium contents were indicative of much shorter average residence times (Fig. 8c). Previous investigations indicated that the Warmbad warm spring may be more strongly affected by admixture of a "young" water component, with average residence times of $\leq$ 40 years (von Storch, 1998). According to von Storch (1998), this fraction is about 18% at Warmbad as opposed to only 7% at Georgsquelle. The absence of dilution of the Warmbad thermal water either suggests that the admixture of water with a lower average residence time must have occurred during recharge or that residence times in the Warmbad geothermal reservoir are shorter by comparison to those of the Georgsquelle reservoir. A likely explanation is that the Warmbad geothermal system is hydraulically more open than the Georgsquelle geothermal system due to being focused along the Warmbad-Chomutov fault system whose trace is continuously exposed at the surface over the entire length from the recharge area to the warm spring.

Both the Warmbad and Georgsquelle thermal waters are characterized by high relative contents of Na and HCO_3, with the Georgsquelle thermal water being more strongly dominated by these dissolved species than the Warmbad thermal water (Fig. 2). The formation of Na-HCO_3 type thermal water has previously been described in a number of other locations worldwide through a combination of increased CO_2 input, plagioclase hydrolysis and, in some cases, cation exchange and calcite formation (Banks and Frengstad, 2006; Chae et al., 2006; Jeong et al., 2005; Marques et al., 2006). The $\delta^{13}C$ ratios of dissolved CO_2 in thermal water are -13 ± 0.7 ‰ at Warmbad and −10.4 ± 0.6 ‰ at Georgsquelle (Prause et al., 2026), suggesting an origin in thermometamorphic CO_2 release from organic-rich sediments, such as metapelites, and inorganic carbonates at depth (Hoefs, 2009). Fault-bound migration would have allowed released CO_2 to come into contact with the geothermal reservoir, where it would have interacted with water, resulting in the formation of carbonic acid:

$$CO_2(g) + H_2O \rightleftharpoons 2H_2CO_3 \quad (8)$$

This in turn would promote the breakdown of plagioclase and alkali feldspars, leading to the accumulation of Na, K, Ca and H_4SiO_4 in solution and producing alkalinity in the form of HCO_3, as exemplified by the following reaction equations:

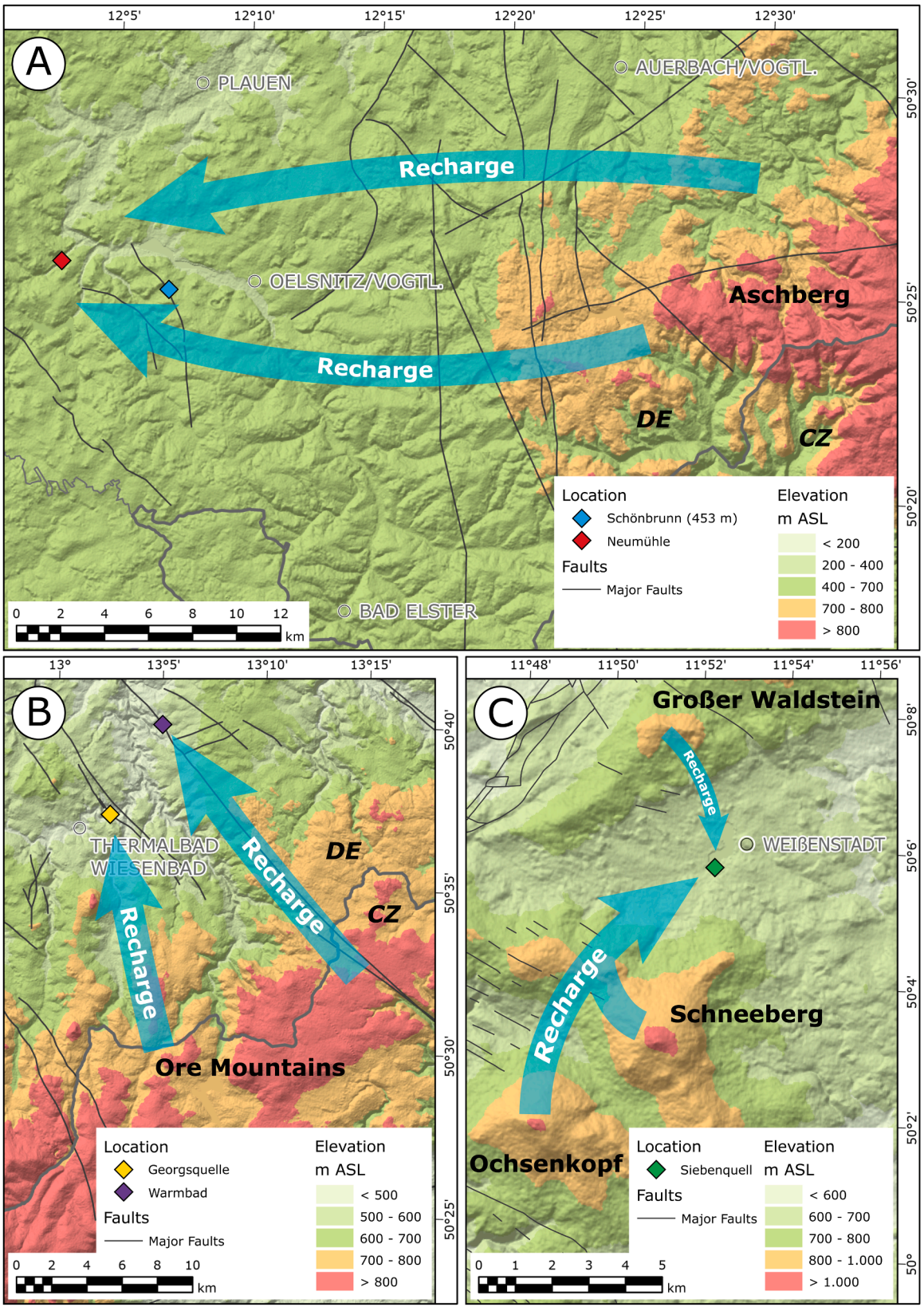

Fig. 9. Overview of most likely recharge areas and flow paths of the geothermal systems at A) Neumühle and Schönbrunn, B) Georgsquelle and Warmbad and C) Siebenquell.

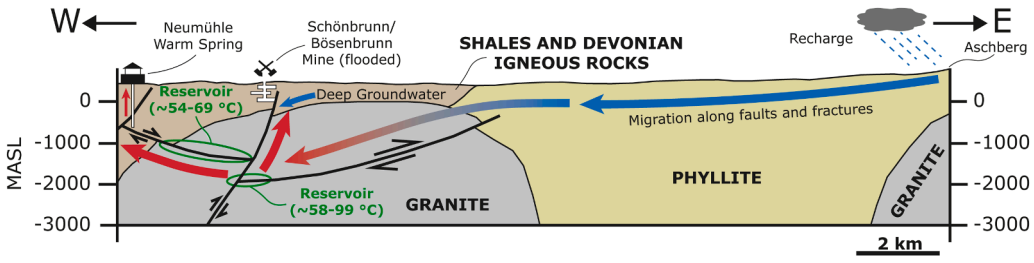

Fig. 10. Simplified conceptual model for the geothermal system producing the thermal waters of the SW-Vogtland region. Recharge occurs at Aschberg at a topographic elevation of ~843–868 m above sea level (MASL). Groundwater migration in phyllite occurs primarily along permeable faults and fractures connected to regional swarm seismicity (e.g., Sonnabend et al., 2023) before infiltrating the concealed granite massif of Eichigt-Schönbrunn and equilibrating with a reservoir at ~2.6 km depth below the surface at temperatures of ~58–99 °C. Rapid upwards migration of thermal water from this reservoir occurs along the steep permeable NW-SE to NNW-SSE striking fault system uncovered in 1973 during mining activity on the 453 m level of the Schönbrunn/Bösenbrunn fluorite mine. Deep non-thermal groundwater mixes with uprising thermal water along the upflow zone. A portion of the deep thermal water re-equilibrates with a shallower reservoir at ~1.8 km depth below the surface, where temperatures range between ~54–69 °C. Thermal water from this reservoir reaches the surface through a separate permeable fault system connected to the Neumühle warm spring without undergoing significant dilution by non-thermal groundwater.

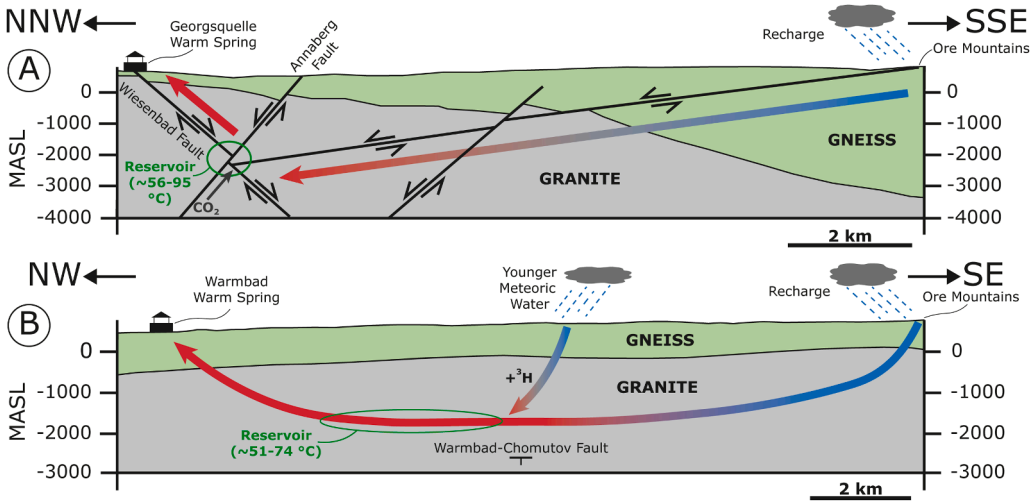

Fig. 11. Simplified conceptual model for the geothermal systems producing the thermal waters of the Central Ore Mountains. A) Recharge of the Georgsquelle geothermal system occurs in the Ore Mountains at a topographic elevation of ~758 m above sea level (MASL). Infiltrating water migrates along a system of permeable faults into the granite hosted geothermal reservoir at ~2.7 km depth. Reservoir temperatures range between ~56–95 °C. The additional input of CO_2 along deep reaching faults enriches the water in carbonic acid and promotes the breakdown of Na-rich plagioclase, giving the Georgsquelle thermal water its distinct Na-HCO_3 character. Reacted thermal water from the reservoir migrates upwards towards the Georgsquelle warm spring along the Wiesenbad Fault System. B) The Warmbad geothermal system likewise recharges in the Ore Mountains at a topographic elevation of ~757 m above sea level (MASL). Migration of thermal water is focused along the Warmbad-Chomutov fault zone, striking parallel to the shown profile. This circulation system is hydraulically more open compared to the Georgsquelle system, enabling the infiltration of younger meteoric water along the flowpath to the reservoir, thereby adding tritium. Thermal water equilibrates with the reservoir at a depth of ~2.3 km below the surface, where temperatures are ~51–74 °C, before reaching the Warmbad warm spring.

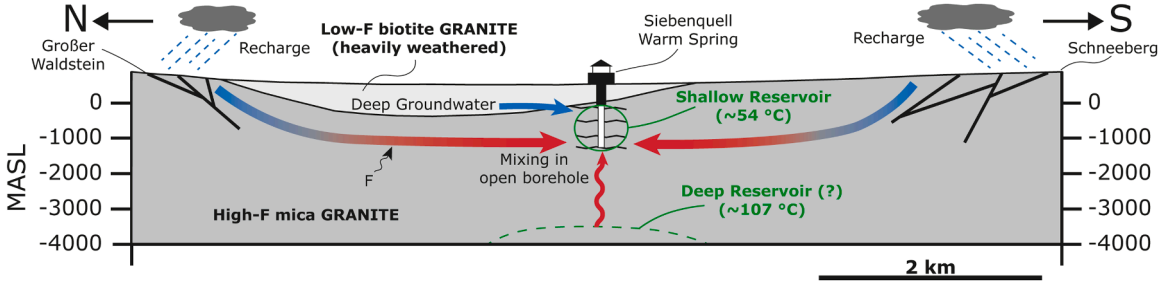

Fig. 12. Simplified conceptual model for the geothermal system producing the Siebenquell thermal water. The system is recharged both to the North and South of the Siebenquell warm spring at Großer Waldstein, Schneeberg and Ochsenkopf (not shown) along permeable faults and fractures. Infiltrating water is enriched in F due to interaction with local high-F mica granites at elevated temperatures. Waters from different depths, including deep non-thermal groundwater, flow into the ~1.8 km deep open Siebenquell borehole along fault-bound permeable inflow zones at depths of ~682–689 m, ~1041–1059 m, ~1450–1562 m and ~1821–1831 m below the surface (Röckel and Stober, 2017). A possible contribution of a deeper reservoir at ~3.8 km below the surface where temperatures are up to ~107 °C is indicated by results from the silica enthalpy mixing model and MEG. The resulting mixed water re-equilibrates in the Siebenquell borehole at temperatures of ~54 °C before reaching the Siebenquell warm spring.

$$2NaAlSi_3O_{8(albite)} + 2H_2CO_3 + 9H_2O \rightarrow Al_2Si_2O_5(OH)_{4(kaolinite)} + 2Na^+ + 2HCO_3^- + 4H_4SiO_4 \quad (9)$$

$$CaAl_2Si_2O_{8(anorthite)} + 2H_2CO_3 + H_2O \rightarrow Al_2Si_2O_5(OH)_{4(kaolinite)} + Ca^{2+} + 2HCO_3^- \quad (10)$$

$$2KAlSi_3O_{8(Kfsp)} + 2H_2CO_3 + 9H_2O \rightarrow Al_2Si_2O_5(OH)_{4(kaolinite)} + 2K^+ + 2HCO_3^- + 4H_4SiO_4 \quad (11)$$

Considering the generally poor solubility of Si, excess silicic acid would be expected to lead to secondary quartz or chalcedony precipitation according to the reaction:

$$H_4SiO_4 \rightarrow SiO_{2(quartz\ or\ chalcedony)} + 2H_2O \quad (12)$$

Plagioclase composition in granitic reservoirs can be expected to be overall more sodic rather than calcic and hence the release of Na (Eq. (9)) may outweigh that of Ca (Eq. (10)). If any breakdown of Ca-rich plagioclase occurred, the accumulation of dissolved Ca could be balanced out to some extent by simultaneous precipitation of calcite, facilitated by high alkalinity:

$$Ca^{2+} + 2HCO_3^- \rightarrow CaCO_{3(calcite)} + CO_2 + H_2O \quad (13)$$

Hence, Ca accumulation in the reacting geothermal fluid from anorthite breakdown may be negligible or less than the accumulation of Na from the dissolution of albite, thereby causing the geothermal fluid to evolve towards a Na-HCO_3 type. Evidence for this process can be found in the low Cl/Na ratios and high SiO_2 concentrations of the Georgsquelle warm spring (Table 2), which suggests that dissolved Na primarily originates from silicate breakdown as opposed to NaCl dissolution or brine input. A lack of evidence for pH changes due to CO_2 degassing in the Warmbad and Georgsquelle thermal waters suggests that CO_2 remains chemically rather than physically dissolved during the ascent to the surface, which may be facilitated by enhanced alkalinity. The higher Na and HCO_3 concentrations of the Georgsquelle thermal water compared to the Warmbad thermal water are therefore interpreted as being due to elevated CO_2 supply and enhanced granite weathering, likely further promoted by the comparatively higher reservoir temperatures and residence times in the Georgsquelle geothermal system.

5.3.3. *Siebenquell*

Because the Siebenquell borehole was not directly accessible, all analyzed thermal water had already cooled down to ~32 °C under surface conditions prior to sampling. This may have caused changes in redox state, pH and major element composition, e.g., via mineral precipitation. In addition, the Siebenquell geothermal system was tapped fairly recently by a deep drilling project in October to December 2013 and pumping tests between 2013 and 2014 recorded highly variable fluid compositions as a function of both time and depth (Röckel and Stober, 2017). It is therefore possible that the system was still in the process of undergoing re-equilibration during our 2022–2024 field survey, which would explain the observed fluctuations in fluid composition, such as highly variable K concentrations, preventing the use of empirical geothermometers except for the silica geothermometer. The combination of these factors complicates the assessment of reservoir conditions at Siebenquell based on presently available data.

The Siebenquell geothermal system recharges from a topographic elevation of ~754 MASL, identifying the nearby granite plateau of Großer Waldstein to the north and the Schneeberg and Ochsenkopf mountains to the south as the most likely recharge areas. The chalcedony geothermometer predicts a temperature of ~54 °C at Siebenquell, which is a near perfect match with the temperature of 53 °C at which the thermal water emerges from the well and the measured temperature of 53.4 °C at the bottom of the Siebenquell borehole (Röckel and Stober, 2017). MEG modeling indicates a dual distribution of equilibrium minerals at both ~85 and ~107 °C (Fig. 6e), with the latter temperature being supported by the results of the silica enthalpy mixing model. The dual distribution of equilibrium minerals at different temperatures in the MEG model may suggest re-equilibration of thermal water from a hotter deeper reservoir with a relatively colder reservoir during ascent to the surface. Additionally, significant degassing of 1.5 mmol $CO_2 \cdot kgw^{-1}$ appears to have occurred in the Siebenquell thermal water between the reservoir(s) and the point of sampling (Fig. 6e), most likely during the above-mentioned time delay between the thermal water reaching the surface and the sample being obtained. This also explains the significantly more alkaline pH of the Siebenquell thermal water compared to the other thermal waters analyzed in this study (Table 4).

Very low tritium contents and high F concentrations in the Siebenquell thermal water as well as its Na-Cl character are the product of extensive water-rock interaction at elevated temperatures in a deep, relatively isolated granitic reservoir. Results of MEG and the silica enthalpy mixing model suggested extensive mixing and dilution of deep hot thermal water with shallower groundwater (Figs. 6e and 7d). The borehole at Siebenquell is cemented between 0–325 m and a packer is installed beneath this depth to ensure that the water reaching the surface is sourced from depths > 580 m (Röckel and Stober, 2017). It follows that mixing between different ground- and thermal waters may have occurred along the primarily fault-bound inflow zones into the uncased well at depths of ~682–689 m, ~1041–1059 m, ~1450–1562 m and ~1821–1831 m (Röckel and Stober, 2017). Given these relatively great depths, the diluting component may have been groundwater with a long average residence time, which is consistent with the low tritium contents in the Siebenquell thermal water (Fig. 8c).

6. Conclusions

The Western Bohemian Massif hosts a regionally developed yet underexplored geothermal resource potentially suitable for direct use applications. A systematic analysis of local warm spring waters indicates that the regional geothermal systems are recharged by meteoric water and typically have reservoir temperatures of < 100 °C, together defining a coherent class of fault-controlled low-enthalpy hot-water type systems. Circulation between the surface and the local radiogenically heated granitic reservoirs at ~2–4 km depth is focused along persistent permeable fault networks.

Hydrochemical variations between individual thermal waters primarily reflect structural differences between regional geothermal systems rather than differences in reservoir lithology, temperature or nature of the heat source. The highly mineralized Cl-rich and tritium depleted thermal waters of the SW-Vogtland region (Neumühle and Schönbrunn) originate from structurally isolated reservoirs receiving minimal recharge from modern precipitation. By contrast, the more hydraulically open geothermal systems in the Central Ore Mountains (Warmbad and Georgsquelle) produce less equilibrated bicarbonate waters of intermediate mineralization and, in the case of Warmbad, detectable tritium, reflecting faster recharge and turnover rates. The Siebenquell thermal water is the product of complex mixing and re-equilibration processes initiated by the intersection of the uncased borehole with multiple permeable fault systems, highlighting the effects of structural complexities when estimating reservoir conditions. Taken together, these findings demonstrate that hydraulic connectivity plays a key role in controlling the hydrochemistry of warm spring water originating from low-enthalpy geothermal systems hosted in crystalline basement rock.

CRediT authorship contribution statement

Simon Prause: Writing – review & editing, Writing – original draft, Visualization, Validation, Methodology, Investigation, Formal analysis,

Data curation, Conceptualization. **Horst Kämpf:** Writing – review & editing, Writing – original draft, Resources, Funding acquisition, Data curation, Conceptualization. **Gerhard Strauch:** Writing – review & editing, Resources, Funding acquisition, Data curation. **Alena Sophie Broge:** Writing – review & editing, Data curation. **Ferdinand Perssen:** Data curation. **Jessica Alexandra Stammeier:** Writing – review & editing. **Sascha Görne:** Visualization, Project administration, Funding acquisition.

Declaration of competing interest

The authors declare that they have no known competing financial interests or personal relationships that could have appeared to influence the work reported in this paper.

Acknowledgements

This study was supported by funding from the Saxon State Office for Environment, Agriculture and Geology (Sächsisches Landesamt für Umwelt, Landwirtschaft und Geologie, LfULG). We would like to thank our editor Sadiq Zarrouk for the handling of our manuscript. Two anonymous reviewers contributed valuable feedback that helped to improve this study. Christian Kunze of the IAF Radioökologie GmbH, Radeberg and the staff of the Hydroisotop GmbH, Schweitenkirchen are credited for the $\delta^{18}O/\delta^{2}H$ and ^{3}H analyses of samples from the 2022–2024 GFZ field survey. Kristin Günther and Sabine Tonn of the Elements and Minerals of the Earth (ElMiE) Laboratory at GFZ Potsdam are thanked for IC/ICP-OES analyses of major dissolved anions and cations for samples collected during the 2022–2024 GFZ field survey. Karina Hemmerling and Manuela Voßberg from Umweltbüro GmbH Weischlitz provided assistance during fieldwork.

Data on the isotopic composition of rainwater from the DWD weather station in Hof were collected by the German Federal Institute for Geosciences and Natural Resources (Bundesanstalt für Geowissenschaften und Rohstoffe, BGR, Hannover) and the German Federal Institute of Hydrology (Bundesanstalt für Gewässerkunde, BfG, Koblenz) and made available for this study by Paul Königer and Axel Schmidt. Kurt von Storch is thanked for his feedback on datasets from his doctoral dissertation relating to the thermal waters included in this work. Additional legacy data for the Geilsdorf Deep Well, the Radonquelle spring in Weißenstadt and thermal waters of the Georgsquelle, Warmbad and Siebenquell warm springs were contributed by Ronny Röder, Ricarda Lorenz, Knut Hinkel and Stephan Gesell. Günther Just, Michael Bauernfeind, Knut Sternitzky, Joachim Petzold and the team of Zweckverband Wasser und Abwasser Vogtland Plauen are thanked for assistance during sampling and additional feedback on legacy data.

Supplementary materials

Supplementary material associated with this article can be found, in the online version, at doi:10.1016/j.geothermics.2026.103677.

Data availability

All data used in this article are available as a separate open access data publication by GFZ Data Services.

References

Agemar, T., Weber, J., Schulz, R., 2014a. Deep geothermal energy production in Germany. Energies 7 (7), 4397–4416. https://doi.org/10.3390/en7074397.

Agemar, T., Alten, J., Ganz, B., Kuder, J., Kühne, K., 2014b. The geothermal information system for Germany-GeotIS. ZDGG 165, 129–144.

Agemar, T., Schellschmidt, R., Schulz, R., 2012. Subsurface temperature distribution in Germany. Geothermics 44, 65–77. https://doi.org/10.1016/j.geothermics.2012.07.002.

Alçiçek, H., Bülbül, A., Brogi, A., Liotta, D., Ruggieri, G., Capezzuoli, E., Meccheri, M., Yavuzer, İ., Alçiçek, M.C., 2018. Origin, evolution and geothermometry of the thermal waters in the Gölemezli Geothermal Field, Denizli Basin (SW Anatolia, Turkey). J. Volcanol. Geotherm. Res. 349, 1–30. https://doi.org/10.1016/j.jvolgeores.2017.07.021.

Andreani, L., Stanek, K.P., Gloaguen, R., Krentz, O., Domínguez-González, L., 2014. DEM-based analysis of interactions between tectonics and landscapes in the Ore Mountains and Eger Rift (East Germany and NW Czech Republic). Remote Sens 6 (9), 7971–8001. https://doi.org/10.3390/rs6097971.

Arnórsson, S., 1975. Application of the stability geothermometer in low temperature hydrothermal areas in Iceland. Amer. J. Sci. 275 (7), 763–784. https://doi.org/10.2475/ajs.275.7.763.

Arnórsson, S., 1989. Deposition of calcium carbonate minerals from geothermal waters - theoretical considerations. Geothermics (1/2), 33–39. https://doi.org/10.1016/0375-6505(89)90007-2.

Arnórsson, S., Gunnlaugsson, E., Svavarsson, H., 1983. The chemistry of geothermal waters in Iceland. III. Chemical geothermometry in geothermal investigations. Geochim. Cosmochim. Acta 47 (3), 567–577. https://doi.org/10.1016/0016-7037(83)90278-8.

Banks, D., Frengstad, B., 2006. Evolution of groundwater chemical composition by plagioclase hydrolysis in Norwegian anorthosites. Geochim. Cosmochim. Acta 70 (6), 1337–1355. https://doi.org/10.1016/j.gca.2005.11.025.

Bankwitz, P., Schneider, G., Kämpf, H., Bankwitz, E., 2003. Structural characteristics of epicentral areas in Central Europe: study case Cheb Basin (Czech Republic). J. Geodyn. 35 (1–2), 5–32. https://doi.org/10.1016/S0264-3707(02)00051-0.

Blasco, M., Auqué, L.F., Gimeno, M.J., 2017. Application of different geothermometrical techniques to a low enthalpy thermal system. Procedia Earth Planet. Sci. 17, 65–68. https://doi.org/10.1016/j.proeps.2016.12.034.

Bräuer, K., Kämpf, H., Koch, U., Strauch, G., 2011. Monthly monitoring of gas and isotope compositions in the free gas phase at degassing locations close to the Nový Kostel focal zone in the western Eger Rift, Czech Republic. Chem. Geol. 290 (3–4), 163–176. https://doi.org/10.1016/j.chemgeo.2011.09.012.

Bräuer, K., Kämpf, H., Niedermann, S., Strauch, G., Tesar, J., 2008. Natural laboratory NW Bohemia: comprehensive fluid studies between 1992 and 2005 used to trace geodynamic processes. Geochem. Geophys. Geosyst. 9 (4), 1–30. https://doi.org/10.1029/2007GC001921.

Bräuer, K., Kämpf, H., Strauch, G., Weise, S.M., 2003. Isotopic evidence (3He/4He, 13CCO2) of fluid-triggered intraplate seismicity. J. Geophys. Res. Solid Earth 108 (B2), 1–11. https://doi.org/10.1029/2002JB002077.

Browne, P.R.L., 1978. Hydrothermal alteration in active geothermal fields. Ann. Rev. Earth Planet. Sci. 6, 229–250.

Burisch, M., Gerdes, A., Meinert, L.D., Albert, R., Seifert, T., Gutzmer, J., 2019. The essence of time – fertile skarn formation in the Variscan Orogenic Belt. Earth Planet. Sci. Lett. 519, 165–170. https://doi.org/10.1016/j.epsl.2019.05.015.

Burisch, M., Markl, G., Gutzmer, J., 2022. Breakup with benefits - hydrothermal mineral systems related to the disintegration of a supercontinent. Earth Planet. Sci. Lett. 580, 117373. https://doi.org/10.1016/j.epsl.2022.117373.

Chae, G.T., Yun, S.T., Kim, K., Mayer, B., 2006. Hydrogeochemistry of sodium-bicarbonate type bedrock groundwater in the Pocheon spa area, South Korea: water–rock interaction and hydrologic mixing. J. Hydrol. 321 (1–4), 326–343. https://doi.org/10.1016/j.jhydrol.2005.08.006.

Chen, L., Zhang, J., Xu, L., Chen, S., Li, Q., Sun, Y., Li, J., Zhao, X., 2024. A study on the geothermal circulation system of granite: an example from the Lancang area, Yunnan. Geothermics 116. https://doi.org/10.1016/j.geothermics.2023.102853.

Collett, S., Schulmann, K., Štípská, P., Míková, J., 2020. Chronological and geochemical constraints on the pre-variscan tectonic history of the Erzgebirge, Saxothuringian Zone. Gondwana Res. 79, 27–48. https://doi.org/10.1016/j.gr.2019.09.009.

Cosmo, R.d.P., Pereira, F.d.A.R., Soares, E.J., Ferreira, E.G., 2022. Addressing the root cause of calcite precipitation that leads to energy loss in geothermal systems. Geothermics 98, 102272. https://doi.org/10.1016/j.geothermics.2021.102272.

Craig, H., 1961. Isotopic variations in meteoric waters. Science 133 (3465), 1702–1703. https://doi.org/10.1126/science.133.3465.1702.

de Wall, H., Schaarschmidt, A., Kämmlein, M., Gabriel, G., Bestmann, M., Scharfenberg, L., 2019. Subsurface granites in the Franconian Basin as the source of enhanced geothermal gradients: a key study from gravity and thermal modeling of the Bayreuth Granite. Int. J. Earth. Sci. 108 (6), 1913–1936. https://doi.org/10.1007/s00531-019-01740-8.

Dill, H.G., Kolb, J., 2019. Carbonate-related metallic and non-metallic mineralization within and proximal to granites (Fichtelgebirge Pluton, Germany): "mantle-crust marker mineralization". Ore Geol. Rev. 104, 46–71. https://doi.org/10.1016/j.oregeorev.2018.10.011.

Ellis, A.J., 1970. Quantitative interpretation of chemical characteristics of hydrothermal systems. Geothermics 2 (3), 516–528. https://doi.org/10.1016/0375-6505(70)90050-7.

Ellis, A.J., 1979. Chemical geothermometry in geothermal systems. Chem. Geol. 25 (3), 219–226. https://doi.org/10.1016/0009-2541(79)90143-8.

Fischer, T., Horálek, J., Hrubcová, P., Vavryčuk, V., Bräuer, K., Kämpf, H., 2014. Intra-continental earthquake swarms in West-Bohemia and Vogtland: a review. Tectonophysics 611, 1–27. https://doi.org/10.1016/j.tecto.2013.11.001.

Förster, A., Förster, H.-J., Krentz, O., 2018. Exploration of the enhanced geothermal system (EGS) potential of crystalline rocks for district heating (Elbe Zone, Saxony, Germany). Int. J. Earth. Sci. 107 (1), 89–101. https://doi.org/10.1007/s00531-016-1429-6.

Förster, A., Förster, H.J., 2000. Crustal composition and mantle heat flow: implications from surface heat flow and radiogenic heat production in the Variscan Erzgebirge (Germany). J. Geophys. Res. Solid Earth 105 (B12), 27917–27938. https://doi.org/10.1029/2000jb900279.

Förster, H.J., Rhede, D., Hecht, L., 2008. Chemical composition of radioactive accessory minerals: implications for the evolution, alteration, age, and uranium fertility of the Fichtelgebirge granites (NE Bavaria, Germany) N. Jb. Miner. Abh. 182 (2), 161–182. https://doi.org/10.1127/0077-7757/2008/0117.

Fournier, R.O., 1977. Chemical geothermometers and mixing models for geothermal systems. Geothermics 5 (1–4), 41–50. https://doi.org/10.1016/0375-6505(77)90007-4.

Fournier, R.O., 1979. A revised equation for the Na/K geothermometer. GRC Transactions 3, 221–224.

Fournier, R.O., 1981. Application of water geochemistry to geothermal exploration and reservoir engineering. In: Rybach, L., Muffler, L.J.P., Wiley, J. (Eds.), Geothermal Systems: Principles and Case Histories, pp. 109–143.

Fournier, R.O., 1985. The behavior of silica in hydrothermal solutions. In: Berger, B.R., Bethke, P.M. (Eds.), Geology and Geochemistry of Epithermal Systems. Society of Economic Geologists (SEG), 140 Buchanan Street, Chelsea, MI 48118, pp. 45–61. https://doi.org/10.5382/Rev.02.

Fournier, R.O., Potter, R.W., 1979. A magnesium correction for the Na-K-Ca chemical geothermometer; report 78-986. US Geological Survey, Menlo Park, California, CA, USA, 1–24.

Fournier, R.O., Truesdell, A.H., 1970. Chemical indicators of subsurface temperature applied to hot spring waters of Yellowstone National Park, Wyoming, U.S.A. Geothermics 2, 529–535. https://doi.org/10.1016/0375-6505(70)90051-9.

Fournier, R.O., Truesdell, A.H., 1973. An empirical Na-K-Ca geothermometer for natural waters. Geochim. Cosmochim. Acta 37 (5), 1255–1275. https://doi.org/10.1016/0016-7037(73)90060-4.

Fournier, R.O., Truesdell, A.H., 1974. Geochemical indicators of subsurface temperature: part 2, estimation of temperature and fraction of hot water mixed with cold water. Jour. Research U.S. Geol. Survey 2 (3), 263–270.

Fowler, A.P.G., Ferguson, C., Cantwell, C.A., Zierenberg, R.A., McClain, J., Spycher, N., Dobson, P., 2018. A conceptual geochemical model of the geothermal system at Surprise Valley, CA. J. Volcanol. Geotherm. Res. 353, 132–148. https://doi.org/10.1016/j.jvolgeores.2018.01.019.

Franke, W., 1989. Tectonostratigraphic units in the Variscan belt of central Europe. In: Dallmeyer, R.D. (Ed.), Terranes in the Circum-Atlantic Paleozoic Orogens. Geol. Soc. Am. Spec. Pap., pp. 67–90. https://doi.org/10.1130/SPE230-p67.

Franz, M., Barth, G., Zimmermann, J., Budach, I., Nowak, K., Wolfgramm, M., 2018. Geothermal resources of the North German Basin: exploration strategy, development examples and remaining opportunities in mesozoic hydrothermal reservoirs. In: Kilhams, B., Kukla, P.A., Mazur, S., McKie, T., Mijnlieff, H.F., van Ojik, K. (Eds.), Mesozoic Resource Potential in the Southern Permian Basin. Geological Society, London. https://doi.org/10.1144/SP469.11.

Frey, M., Bär, K., Stober, I., Reinecker, J., van der Vaart, J., Sass, I., 2022. Assessment of deep geothermal research and development in the Upper Rhine Graben. Geotherm. Energy 10 (1), 18. https://doi.org/10.1186/s40517-022-00226-2.

Giggenbach, W.F., 1988. Geothermal solute equilibria. Derivation of Na-K-Mg-Ca geoindicators. Geochim. Cosmochim. Acta 52 (12), 2749–2765. https://doi.org/10.1016/0016-7037(88)90143-3.

Giggenbach, W.F., 1991. Chemical techniques in geothermal exploration, application of geochemistry in geothermal reservoir development. pp. 119–144.

Giggenbach, W.F., Goguel, R.L., 1989. Collection and analysis of geothermal and volcanic water and gas discharges. DSIR report CD 2401 Pentone, New Zealand.

Gottesmann, B., Förster, H.-J., Müller, A., Kämpf, H., 2017. The concealed granite massif of Eichigt-Schönbrunn (Vogtland, Germany): petrography, mineralogy, geochemistry and age of the Eichigt apical intrusion. Freiberg Online Geoscience 49, 1–46.

Han, D.M., Liang, X., Jin, M.G., Currell, M.J., Song, X.F., Liu, C.M., 2010. Evaluation of groundwater hydrochemical characteristics and mixing behavior in the Daying and Qicun geothermal systems, Xinzhou Basin. J. Volcanol. Geotherm. Res. 189 (1–2), 92–104. https://doi.org/10.1016/j.jvolgeores.2009.10.011.

Hardie, L.A., 1990. The roles of rifting and hydrothermal CaCl2 brines in the origin of potash evaporites: an hypothesis. Amer. J. Sci. 290 (1), 43–106.

Hecht, L., Vigneresse, J.L., 1999. A multidisciplinary approach combining geochemical, gravity and structural data: implications for pluton emplacement and zonation. In: Castro, A., Fernández, C., Vigneresse, J.L. (Eds.), Understanding Granites: Integrating New and Classical Techniques. Geol. Soc. Lond. Spec. Publ., pp. 95–110. https://doi.org/10.1144/GSL.SP.1999.168.01.07

Hloušek, F., Hellwig, O., Buske, S., 2015. Three-dimensional focused seismic imaging for geothermal exploration in crystalline rock near Schneeberg, Germany. Geophys. Prospect. 63 (4), 999–1014. https://doi.org/10.1111/1365-2478.12239.

Hoefs, J., 2009. Stable Isotope Geochemistry. Springer, Berlin, Heidelberg. https://doi.org/10.1007/978-3-540-70708-0.

Hofmann, K., Görz, I., Riedel, P., Heiermann, M., Franěk, J., Jelének, J., Holeček, J., 2021. Erdwärme: harmonisierte Methoden zur potenzialdarstellung. Schriftenreihe des LfULG, Heft 1–77, 7/2021.

Hoth, K., Ossenkopf, W., Hösel, G., Zernke, B., Eisenschmidt, K., Kühne, R., 1991. Die Granite im westteil des Mittelerzgebirgischen Teilplutons und ihr Rahmen. Geoprofil 3, 3–13.

Hou, Z., Xu, T., Li, S., Jiang, Z., Feng, B., Cao, Y., Feng, G., Yuan, Y., Hu, Z., 2019. Reconstruction of different original water chemical compositions and estimation of reservoir temperature from mixed geothermal water using the method of integrated multicomponent geothermometry: a case study of the Gonghe Basin, northeastern Tibetan Plateau, China. Appl. Geochem. 108, 104389. https://doi.org/10.1016/j.apgeochem.2019.104389.

Jeong, C.H., Kim, H.J., Lee, S.Y., 2005. Hydrochemistry and genesis of CO2-rich springs from mesozoic granitoids and their adjacent rocks in South Korea. Geochem. J. 39 (6), 517–530. https://doi.org/10.2343/geochemj.39.517.

Kämpf, H., Geissler, W.H., Bräuer, K., 2007. Combined gas-geochemical and receiver function studies of the Vogtland/NW Bohemia Intraplate Mantle degassing Field, Central Europe. In: Ritter, J.R.R., Christensen, U.R. (Eds.), Mantle plumes: A Multidisciplinary Approach. Springer, Berlin, Heidelberg, pp. 127–158. https://doi.org/10.1007/978-3-540-68046-8_4.

Kämpf, H., 1982. Minerogenie Hydrothermaler Gangmineralisationen am Beispiel eines Fluorit-Lagerstättenreviers im Vogtland 8DDR. Bergakademie Freiberg, Freiberg. Doctoral Dissertation.

Kaya, T., Hoşhan, P., 2005. Corrosion and material selection for geothermal systems. In: Proceedings World Geothermal Congress. Antalya, Turkey, pp. 1–5.

Kroner, U., Hahn, T., Romer, R.L., Linnemann, U., 2007. The variscan orogeny in the saxo-thuringian zone - heterogenous overprint of cadomian/palaeozoic Peri-Gondwana crust. In: Linnemann, U., Nance, R.D., Kraft, P., Zulauf, G. (Eds.), The Evolution of the Rheic Ocean: From Avalonian-Cadomian Active Margin to Alleghenian-Variscan Collision. Geol. Soc. Am. Spec. Pap., pp. 153–172. https://doi.org/10.1130/2007.2423(06)

Kuschka, E., 1997. Atlas Der Hydrothermalite Des Vogtlandes, Erzgebirges und Granulitgebirges. Sächsisches Landesamt Für Umwelt und Geologie. Bereich Boden und Geologie.

Kuschka, E., 2002. Zur Tektonik, Verbreitung und minerogenie sächsischer hydrothermaler mineralgänge. Geoprofil 11, 1–186.

Li, J., Sagoe, G., Li, Y., 2020. Applicability and limitations of potassium-related classical geothermometers for crystalline basement reservoirs. Geothermics 84. https://doi.org/10.1016/j.geothermics.2019.101728.

Li, J., Sagoe, G., Yang, G., Lu, G., 2018. Evaluation of mineral-aqueous chemical equilibria of felsic reservoirs with low-medium temperature: a comparative study in Yangbajing geothermal field and Guangdong geothermal fields. J. Volcanol. Geotherm. Res. 352, 92–105. https://doi.org/10.1016/j.jvolgeores.2018.01.008.

Li, Y., Pan, T., Li, H., Cheng, H., Zhang, P., Han, W., Li, B., Yuan, Q., Ma, X., Ma, H., 2024. Source and genesis of Ca-Cl type brines in Qaidam Basin, Qinghai-Tibetan Plateau: evidence from hydrochemistry as well as B and Li isotopes. Front. Environ. Sci. 11, 1248294. https://doi.org/10.3389/fenvs.2023.1248294.

Lowenstein, T.K., Risacher, F., 2009. Closed Basin brine evolution and the influence of Ca–Cl inflow waters: death Valley and Bristol Dry Lake California, Qaidam Basin, China, and Salar de Atacama, Chile. Aquat. Geochem. 15 (1–2), 71–94. https://doi.org/10.1007/s10498-008-9046-z.

Lüschen, E., Görne, S., von Hartmann, H., Thomas, R., Schulz, R., 2015. 3D seismic survey for geothermal exploration in crystalline rocks in Saxony, Germany. Geophys. Prospect. 63 (4), 975–989. https://doi.org/10.1111/1365-2478.12249.

Lüschen, E., Schulz, R., 2014. 3-D seismic surveys explore German petrothermal reserves. Eos Trans. Am. Geophys. Union 95 (26), 237–238. https://doi.org/10.1002/2014eo260001.

Mao, X., Dong, Y., He, Y., Zhu, D., Shi, Z., Ye, J., 2022. The effect of granite fracture network on silica-enriched groundwater formation and geothermometers in low-temperature hydrothermal system. J. Hydrol. 609, 127720. https://doi.org/10.1016/j.jhydrol.2022.127720.

Mao, X., Zhu, D., Ndikubwimana, I., He, Y., Shi, Z., 2021. The mechanism of high-salinity thermal groundwater in Xinzhou geothermal field, South China: insight from water chemistry and stable isotopes. J. Hydrol. 593, 125889. https://doi.org/10.1016/j.jhydrol.2020.125889.

Marques, J.M., Andrade, M., Carreira, P.M., Eggenkamp, H.G.M., Graça, R.C., Aires-Barros, L., Antunes Da Silva, M., 2006. Chemical and isotopic signatures of Na/HCO3/CO2-rich geofluids, North Portugal. Geofluids 6 (4), 273–287. https://doi.org/10.1111/j.1468-8123.2006.00144.x.

Marques, J.M., Espinha Marques, J., Carreira, P.M., Graça, R.C., Aires-Barros, L., Carvalho, J.M., Chaminé, H.I., Borges, F.S., 2003. Geothermal fluids circulation at Caldas do Moledo area, Northern Portugal: geochemical and isotopic signatures. Geofluids 3 (3), 189–201. https://doi.org/10.1046/j.1468-8123.2003.00059.x.

Michard, G., 1990. Behaviour of major elements and some trace elements (Li, Rb, Cs, Sr, Fe, Mn, W, F) in deep hot waters from granitic areas. Chem. Geol. 89 (1–2), 117–134. https://doi.org/10.1016/0009-2541(90)90062-C.

Mingram, B., 1998. The Erzgebirge, Germany, a subducted part of northern Gondwana: geochemical evidence for repetition of early palaeozoic metasedimentary sequences in metamorphic thrust units. Geol. Mag 135 (6), 785–801. https://doi.org/10.1017/S0016756898001769.

Moeck, I.S., Dussel, M., Weber, J., Schintgen, T., Wolfgramm, M., 2019. Geothermal play typing in Germany, case study Molasse Basin: a modern concept to categorise geothermal resources related to crustal permeability. Neth. J. Geosci. 98, e14. https://doi.org/10.1017/njg.2019.12.

Morey, G.W., Fournier, R.O., Rowe, J.J., 1962. The solubility of quartz in water in the temperature interval from 25° to 300 °C. Geochim. Cosmochim. Acta 26 (10). https://doi.org/10.1016/0016-7037(62)90027-3.

Mrlina, J., Kämpf, H., Kroner, C., Mingram, J., Stebich, M., Brauer, A., Geissler, W.H., Kallmeyer, J., Matthes, H., Seidl, M., 2009. Discovery of the first quaternary maar in the Bohemian Massif, Central Europe, based on combined geophysical and geological surveys. J. Volcanol. Geotherm. Res. 182 (1–2), 97–112. https://doi.org/10.1016/j.jvolgeores.2009.01.027.

Murray, H.H., 1988. Kaolin minerals: their genesis and occurrences. In: Bailey, S.W. (Ed.), Hydrous Phyllosilicates (exclusive of Micas). Mineralogical Society of America, Washington, D.C., pp. 67–89

Ngo, V.V., Lucas, Y., Clément, A., Fritz, B., 2016. Modeling the impact of temperature on the saturation state and behavior of minerals in the Soultz-sous-Forêts geothermal system. Geothermics 64, 196–208. https://doi.org/10.1016/j.geothermics.2016.06.001.

Nicholson, K.N., 1993. Geothermal Fluids: Chemistry and Exploration Techniques. Springer-Verlag, Berlin, Heidelberg, New York, London, Paris, Tokyo, Hong Kong. https://doi.org/10.1017/S0016756800011535.
Nieva, D., Nieva, R., 1987. Developments in geothermal energy in Mexico - part twelve. A cationic geothermometer for prospecting of geothermal resources. Heat Recovery Systems and CHP 7 (3), 243–258. https://doi.org/10.1016/0890-4332(87)90138-4.
Nogara, J., Zarrouk, S.J., 2018. Corrosion in geothermal environment: part 1: fluids and their impact. Renew. Sustain. Energy Rev. 82, 1333–1346. https://doi.org/10.1016/j.rser.2017.06.098.
Palandri, J.L., Reed, M.H., 2001. Reconstruction of in situ composition of sedimentary formation waters. Geochim. Cosmochim. Acta 65 (11), 1741–1767. https://doi.org/10.1016/S0016-7037(01)00555-5.
Pang, Z.H., Reed, M.H., 1998. Theoretical chemical thermometry on geothermal waters: problems and methods. Geochim. Cosmochim. Acta 62 (6), 1083–1091. https://doi.org/10.1016/S0016-7037(98)00037-4.
Parkhurst, D.L., Appelo, C.A.J., 1999. User's guide to PHREEQC (Version 2): a computer program for speciation, batch-reaction, one-dimensional transport, and inverse geochemical calculations. Water-resources Investig. Rep. U.S. Geological Survey. https://doi.org/10.3133/wri994259.
Parneix, J.C., Petit, J.C., 1991. Hydrothermal alteration of an old geothermal system in the Auriat granite (Massif Central, France): petrological study and modelling. Chem. Geol. 89 (3–4), 329–351. https://doi.org/10.1016/0009-2541(91)90023-K.
Pope, L.A., Hajash, A., Popp, R.K., 1987. An experimental investigation of the quartz, Na-K, Na-K-Ca geothermometers and the effects of fluid composition. J. Volcanol. Geotherm. Res. 31 (1–2), 151–161. https://doi.org/10.1016/0377-0273(87)90012-6.
Prause, S., Kämpf, H., Strauch, G., Broge, A.S., Perssen, F., Kunze, C., Stammeier, J.A., Günther, K., Tonn, S., Görne, S., 2026. Hydrochemical and isotopic dataset for the characterization of fault-bound hydrothermal reservoirs of the Western Bohemian Massif (Germany). GFZ Data Services. https://doi.org/10.5880/GFZ.EXPQ.2026.001.
Reed, M.H., 1982. Calculation of multicomponent chemical equilibria and reaction processes in systems involving minerals, gases and an aqueous phase. Geochim. Cosmochim. Acta 46 (4), 513–528. https://doi.org/10.1016/0016-7037(82)90155-7.
Reed, M.H., Spycher, N., 1984. Calculation of pH and mineral equilibria in hydrothermal waters with application to geothermometry and studies of boiling and dilution. Geochim. Cosmochim. Acta 48 (7), 1479–1492. https://doi.org/10.1016/0016-7037(84)90404-6.
Röckel, L., Stober, I., 2017. Die neue Tiefbohrung Weißenstadt im Granit des Fichtelgebirges. Grundwasser 22 (3), 165–173. https://doi.org/10.1007/s00767-017-0361-4.
Romer, R.L., Thomas, R., Stein, H.J., Rhede, D., 2007. Dating multiply overprinted Sn-mineralized granites—Examples from the Erzgebirge. Germany. Miner. Depos. 42 (4), 337–359. https://doi.org/10.1007/s00126-006-0114-2.
Rötzler, K., Plessen, B., 2010. The Erzgebirge: a pile of ultrahigh-to low-pressure nappes of early palaeozoic rocks and their cadomian basement. In: Linnemann, U., Romer, R.L. (Eds.), Pre-Mesozoic Geology of Saxo-Thuringia - From the Cadomian Active Margin to the Variscan Orogen. Schweizerbart, Stuttgart, pp. 253–270.
Santoyo, E., Díaz-González, L., 2010. A new improved proposal of the Na/K geothermometer to estimate deep equilibrium temperatures and their uncertainties in geothermal systems. In: Proceedings World Geothermal Congress. Bali, Indonesia, pp. 1–9.
Savage, D., Cave, M.R., Milodowski, A.E., George, I., 1987. Hydrothermal alteration of granite by meteoric fluid: an example from the Carnmenellis Granite, United Kingdom. Contrib. Mineral. Petrol. 96, 391–405. https://doi.org/10.1007/BF00371257.
Schäfer, F., Oncken, O., Kemnitz, H., Romer, R.L., 2000. Upper-plate deformation during collisional orogeny: a case study from the German Variscides (Saxo-Thuringian Zone). In: Franke, W., Haak, V., Oncken, O., Tanner, D. (Eds.), Orogenic Processes: Quantification and Modelling in the Variscan Belt. Geol. Soc. Lond. Spec. Pub., pp. 281–302. https://doi.org/10.1144/GSL.SP.2000.179.01.17
Schmidt, A., Frank, G., Stichler, W., Duester, L., Steinkopff, T., Stumpp, C., 2020. Overview of tritium records from precipitation and surface waters in Germany. Hydrol. Process. 34 (6), 1489–1493. https://doi.org/10.1002/hyp.13691.
Schulz, B., Krause, J., 2024. Electron probe petrochronology of monazite- and garnet-bearing metamorphic rocks in the saxothuringian allochthonous domains (Erzgebirge, Granulite and Münchberg massifs). In: van Schijndel, V., Cutts, K., Pereira, I., Guitreau, M., Volante, S., Tedeschi, M. (Eds.), Minor Minerals, Major Implications: Using Key Mineral Phases to Unravel the Formation and Evolution of Earth's Crust. Geol. Soc. Lond. Spec. Pub. https://doi.org/10.1144/SP537-2022-195.
Schützel, H., Hösel, G., 1962. Eine neue mineralquelle im südwestlichen Vogtland und Bemerkungen zum granitmassiv von Eichigt-Schönbrunn. Z. angew. Geol. 8, 404–408.
Schwan, W., 1959. Querschollenbau in einem Teil des Variszischen Gebirges. Geol. Rundsch. 46 (2), 349–371. https://doi.org/10.1007/BF01803030.
Siebel, W., Chen, F., Satir, M., 2003. Late-variscan magmatism revisited: new implications from Pb-evaporation zircon ages on the emplacement of redwitzites and granites in NE Bavaria. Int. J. Earth. Sci. 92, 36–53. https://doi.org/10.1007/s00531-002-0305-8.
Simmons, S.F., 2013. Fluid-mineral equilibria in great basin geothermal systems: implications for chemical geothermometry. In: Proceedings, Thirty-Eighth Workshop on Geothermal Reservoir Engineering. Stanford, California. Stanford University.
Sonnabend, L., Rein, N., Korn, M., 2023. Neotektonik und seismizität in Westsachsen und Nordwestböhmen. Schriftenreihe des Landesamtes für Umwelt, Landwirtschaft und Geologie 8, 1–97.
Stephan, T., Hallas, P., Kroner, U., 2015. 3D modelling of the Variscan granites in the Erzgebirge-Vogtland-Fichtelgebirge area. In: CETEG 2015. Conference Paper.
Stephan, T., Hallas, P., Kirsch, M., Kroner, U., Buske, S., 2018. Crustal-scale 3D modelling of the allochthonous Domain of the Erzgebirge-Vogtland-Fichtelgebirge area, Saxo-Thuringian Zone. In: 17th Symposium of Tectonics, Structural Geology and Crystalline Geology. Conference Paper.
Stumpp, C., Klaus, J., Stichler, W., 2014. Analysis of long-term stable isotopic composition in German precipitation. J. Hydrol. 517, 351–361. https://doi.org/10.1016/j.jhydrol.2014.05.034.
Suchi, E., Dittmann, J., Knopf, S., Müller, C., Schulz, R., 2014. Geothermal Atlas to visualise potential conflicts of interest between CO2 storage (CCS) and deep geothermal energy in Germany. German J. Geosci. 165 (3), 439–453. https://doi.org/10.1127/1860-1804/2014/0070.
Tichomirowa, M., Berger, H.-J., Koch, E.A., Belyatski, B.V., Götze, J., Kempe, U., Nasdala, L., Schaltegger, U., 2001. Zircon ages of high-grade gneisses in the Eastern Erzgebirge (Central European Variscides)—Constraints on origin of the rocks and precambrian to ordovician magmatic events in the Variscan foldbelt. Lithos 56 (4), 303–332. https://doi.org/10.1016/S0024-4937(00)00066-9.
Tichomirowa, M., Käßner, A., Burisch, M., Weber, S., Lehmann, U., Görz, I., 2025. Diachronous pulses of Variscan magmatic activity in the Eastern and Western Erzgebirge (Germany and Czech Republic), their temporal geochemical evolution, and their relation to ore formation. Int. J. Earth. Sci. 114, 531–551. https://doi.org/10.1007/s00531-025-02499-x.
Truesdell, A.H., Fournier, R.O., 1977. Procedure for estimating the temperature of a hot-water component in a mixed water by using a plot of dissolved silica versus enthalpy. Jour. Res. U.S. Geol. Survey 5 (1), 49–52.
Ulrych, J., Dostal, J., Adamovič, J., Jelínek, E., Špaček, P., Hegner, E., Balogh, K., 2011. Recurrent cenozoic volcanic activity in the Bohemian Massif (Czech Republic). Lithos 123 (1–4), 133–144. https://doi.org/10.1016/j.lithos.2010.12.008.
Voigt, M., Marieni, C., Clark, D.E., Gíslason, S.R., Oelkers, E.H., 2018. Evaluation and refinement of thermodynamic databases for mineral carbonation. Energy Procedia 146, 81–91. https://doi.org/10.1016/j.egypro.2018.07.012.
von Storch, K., 1998. Herkunft Der Balneologisch Wertbestimmenden Eigenschaften in Sächsischen Mineral- und Thermalwässern. Fakultät für Physik und Geowissenschaften. Universität Leipzig, Leipzig. Doctoral Dissertation.
von Storch, K., Jordan, H.P., Glässer, W., Abraham, T., Grimm, R., Müller, B., 2000. Mineral und thermalwässer in Sachsen. Geoprofil 9, 1–263.
Vylita, T., Žák, K., Cílek, V., Hercman, H., Mikšíková, L., 2007. Evolution of hot-spring travertine accumulation in Karlovy Vary/Carlsbad (Czech Republic) and its significance for the evolution of Teplá valley and Ohře/Eger rift. Z. Geomorph. 51 (4), 427–442.
Waltgenbach, S., Riechelmann, D.F.C., Spötl, C., Jochum, K.P., Fohlmeister, J., Schröder-Ritzrau, A., Scholz, D., 2021. Climate variability in Central Europe during the last 2500 years reconstructed from four high-resolution multi-proxy speleothem records. Geosciences (Basel) 11 (4), 166. https://doi.org/10.3390/geosciences11040166.
Wang, H., Mao, X., Li, C., Dong, Y., Ye, J., 2023a. An additional source for the hydrochemical formation of geothermal waters in granites. Geothermics 114, 102793. https://doi.org/10.1016/j.geothermics.2023.102793.
Wang, L., Liu, K., Zhang, S., Zhang, Y., Jia, W., Yu, T., Guo, J., 2023b. Estimation of reservoir temperature and analysis of the mechanism of origin of a granite dome-controlled geothermal system in the western Wugongshan area, southeast China. Front. Environ. Sci. 11, 1226074. https://doi.org/10.3389/feart.2023.1226074.
Weber, J., Born, H., Pester, S., Moeck, I.S., 2020. Geothermal energy use in Germany, country update 2015-2019. In: Proceedings World Geothermal Congress. Reykjavik, Iceland.
Weisser, O., De Vleeschouwer, D., Strauss, H., 2024. The influence of climate change on the δ18O and δ2H signatures of meteoric waters in Europe and North America. Model. Earth Syst. Environ. 10, 6917–6930. https://doi.org/10.1007/s40808-024-02137-6.
Winter, T., Aeschbach, W., Einsiedl, F., 2024. Reconstruction of the pleistocene paleoclimate from deep groundwater in southern Germany from noble gas temperatures linked with organic radiocarbon dating. Water Resour. Res. 60 (1), e2023WR035644. https://doi.org/10.1029/2023WR035644.
Xiao, Q., Jiang, Y., Shen, L., Yuan, D., 2018. Origin of calcium sulfate-type water in the triassic carbonate thermal water system in Chongqing, China: a chemical and isotopic reconnaissance. Appl. Geochem. 89, 49–58. https://doi.org/10.1016/j.apgeochem.2017.11.011.
Xu, P., Zhao, M., Fu, X., Zhao, C., 2022. Effect of chloride ions on the corrosion behavior of carbon steel in an iron bacteria system. RSC Adv 12 (24), 15158–15166. https://doi.org/10.1039/d2ra02410a.
Yasuhara, H., Kinoshita, N., Ohfuji, H., Lee, D.S., Nakashima, S., Kishida, K., 2011. Temporal alteration of fracture permeability in granite under hydrothermal conditions and its interpretation by coupled chemo-mechanical model. Appl. Geochem. 26 (12), 2074–2088. https://doi.org/10.1016/j.apgeochem.2011.07.005.
Zhao, M., Yin, F., Xiao, J., Chang, H., Pi, J., Zhou, X., Yao, T., Wang, C., 2023. Hydrogeochemistry and formation of low temperature geothermal waters in South Hunan, China. Geochem. Int. 61 (13), 1382–1393. https://doi.org/10.1134/s0016702923110113.